Biol Cybern (2006) 95: 31–53
DOI 10.1007/s00422-006-0067-7

ORIGINAL PAPER

Biological Cybernetics

Armin Biess · Mark Nagurka · Tamar Flash

Simulating discrete and rhythmic multi-joint human arm movements by optimization of nonlinear performance indices

Received: 9 May 2005 / Accepted: 8 March 2006 / Published online: 13 May 2006

Abstract An optimization approach applied to mechanical linkage models is used to simulate human arm movements. Predicted arm trajectories are the result of minimizing a nonlinear performance index that depends on kinematic or dynamic variables of the movement. A robust optimization algorithm is presented that computes trajectories which satisfy the necessary conditions with high accuracy. It is especially adapted to the analysis of discrete and rhythmic movements. The optimization problem is solved by parameterizing each generalized coordinate (e.g., joint angular displacement) in terms of Jacobi polynomials and Fourier series, depending on whether discrete or rhythmic movements are considered, combined with a multiple shooting algorithm. The parameterization of coordinates has two advantages. First, it provides an initial guess for the multiple shooting algorithm which solves the optimization problem with high accuracy. Second, it leads to a low dimensional representation of discrete and rhythmic movements in terms of expansion coefficients. The selection of a suitable feature space is an important prerequisite for comparison, recognition and classification of movements. In addition, the separate computational analysis of discrete and rhythmic movements is motivated by their distinct neurophysiological realizations in the cortex. By investigating different performance indices subject to different boundary conditions, the approach can be used to examine possible strategies that humans adopt in selecting specific arm motions for the performance of different tasks in a plane and in three-dimensional space.

A. Biess (✉)
Department of Mathematics, The Weizmann Institute of Science, 76100 Rehovot, Israel
E-mail: armin.biess@weizmann.ac.il
Tel.: +972-8-934-3292
Fax: +972-8-934-4309

M. Nagurka
Department of Mechanical and Industrial Engineering, Marquette University, Milwaukee, WI 53201-1881, USA

T. Flash
Department of Computer Science and Applied Mathematics, The Weizmann Institute of Science, 76100 Rehovot, Israel

1 Introduction

The planning and control of human arm movements is of major interest in motor control research. In any motor task, such as pointing, grasping, holding or writing, the repertoire of movements that is used represents a subset of those that are admissible. The physical structure of the human body, such as the kinematic restrictions at the joints, preclude certain motions. The muscles (actuators), the visual and proprioceptive systems (sensors), and the signaling and information processing by neurons within the central nervous system (CNS; the controller) impose further constraints on the movements. It is presumed that among a wide choice of possibilities the CNS implements certain planning strategies leading to the arm movements that are ultimately observed.

Human arm movement planning and control strategies can be investigated by analyzing and measuring the kinematic and dynamic features of arm movements under various conditions and then inferring a general motor strategy from the observed data. A popular approach to investigate the strategies underlying the generation of human arm movements is based on optimization and optimal control theories. The underlying assumption is that the CNS optimizes the performance that can be expressed mathematically in terms of a cost, or a performance index.

Existing optimization principles can be divided into deterministic and stochastic approaches. In a deterministic description the cost is typically expressed as the integral of some deterministic function over the movement time. The minimization of a performance index subject to a set of dynamic equations and suitable boundary conditions leads to the optimal solution which defines the outcome of the theoretical model. Deterministic models can account for the mean properties of the movements and thus constitute a first approximation to the observed motor behavior. The minimum-jerk model (Flash and Hogan 1985) and the minimum torque

change model (Nakano et al. 1999; Uno et al. 1989) are two popular representations.

In a stochastic description, random disturbances (noise) are included in the description and only the expected value of the cost function can be minimized. The minimization of such costs, subject to dynamic equations and suitable boundary conditions, is the subject of stochastic optimal control theory. The minimum-variance model (Harris and Wolpert 1998) and the minimum-intervention model (Todorov and Jordan 2002) are examples of stochastic models.

In this paper, we focus exclusively on models derived from a deterministic cost function. The dominant challenging research question is how to posit a performance index that faithfully predicts the main kinematic and dynamic features of the movement. Many of the indices suggested for studying human motor control problems are nonlinear and their minimization poses a difficult problem. Methods for calculating optimal trajectories in a robust and precise way are indispensable.

This paper presents a method that can be used for the minimization of nonlinear performance indices and the investigation of plausible human motion planning strategies in two- and three-dimensional space. The main goal of the study consists in the development of an algorithm that computes trajectories which satisfy the necessary conditions of optimality with high accuracy. Many previous studies have ignored this problem or not addressed it sufficiently, implying that the derived solutions are not guaranteed to be optimal. It is well known that the solution of the necessary conditions is not guaranteed to be optimal and further conditions have to be specified. Sufficient conditions can be specified but their (numerical) analysis is beyond this scope of the paper.

The computational method proposed here is developed for the study of discrete (point-to-point) and rhythmic movements. As part of the algorithm, a low dimensional representation of discrete and rhythmic movements in terms of a set of expansion coefficients is presented. It is a well-known fact that the selection of a suitable feature space is a necessary prerequisite for the comparison, recognition and classification of movements (Bishop 1995).

Many existing models of human arm movements are based on the minimization of nonlinear cost functions. Uno et al. (1989) applied a Newton-like method to the minimization of the performance index defined by the minimum torque change criterion. A steepest descent method combined with a penalty method for the minimization of the performance index defined by the minimum torque change criterion was used by Nakano et al. (1999). However, these minimization algorithms often diverge and are unstable.

Wada et al. (2001) emphasized the difficulty in computing optimal trajectories and proposed a method to calculate the optimal trajectory for the minimum commanded torque change criteria in a robust way which ensured that the necessary conditions of optimality are satisfied with high accuracy. In that work and a subsequent paper by Kaneko et al. (2005), the joint angles were expanded in terms of orthogonal polynomials and the coefficients were determined by iteratively solving a linearized set of Euler–Lagrange equations. The main drawbacks of that method consist of the tedious task of linearization and the unspecified convergence conditions of the method.

Todorov and Jordan (1998) optimized the minimum-jerk functional along arbitrary given paths by introducing fixed points along the path and solving the resulting nonlinear equations with a Simplex method.

A method for predicting trajectories of a two-link planar robot model that minimized the sum of the square of joint torques was presented by Yen and Nagurka (1988). In their method the angular displacement of each robot joint was approximated by the sum of a polynomial and a finite-term Fourier series. The optimal control problem was thus cast as a parameter optimization problem which was then solved via a Simplex algorithm. In a subsequent paper, Nagurka and Yen (1990) used that approach to generate trajectories of general dynamic systems. In their work, the interest was in determining near optimal trajectories of the generalized coordinates (or state variables) without consideration of the higher time derivatives of the position coordinates nor of the need to satisfy the Euler–Lagrange equations.

Previous studies, with the exception of Wada et al. (2001) and Kaneko et al. (2005), have not addressed the optimization problem sufficiently to ensure that the necessary conditions of optimality are satisfied. This may affect the accuracy of the optimal solution found as the outcome of the computational model.

This work presents a general method for the computation of the optimal solution derived from a performance index that satisfies the necessary condition of optimality to high accuracy. Moreover, the parameterization of coordinates, as part of the algorithm, leads to a novel compact vector representation of discrete and rhythmic movements, which may be used for the definition of motor primitives and may be important for the comparison, recognition and classification of human movements.

2 Methods

Consider a variational problem with a cost functional (performance index) of the form

$$\mathcal{C} = \int_0^{\mathrm{T}} F\left[\mathbf{q}(t), \dot{\mathbf{q}}(t), \ddot{\mathbf{q}}(t), \ldots, \mathbf{q}^{(m)}(t), t\right] \mathrm{d}t, \tag{1}$$

where $\mathbf{q}^{(m)}(t)$ denotes the m-th derivative of the generalized coordinate vector $\mathbf{q}(t) = [q_1(t), q_2(t), \ldots, q_n(t)]^{\mathrm{T}}$ with respect to time for an n degree-of-freedom (DOF) system, and T denotes the total movement time, or in the case of rhythmic movements, the period of the movement. For a human arm, modeled as a mechanical linkage system consisting of serial rigid links, these generalized coordinates are typically chosen to be the angular displacements at the joints or the end-effector coordinates. It is assumed in the following that

the highest derivative appearing in the Lagrangian, F, is quadratic. A large number of cost functionals used in the modeling of human arm movements falls into this class.

A necessary condition to obtain an extremum of the cost functional (1) is given by the Euler–Lagrange equations:

$$E_i = \frac{\partial F}{\partial q_i} - \frac{\mathrm{d}}{\mathrm{d}t}\frac{\partial F}{\partial \dot{q}_i} + \cdots + (-1)^m \frac{\mathrm{d}^m}{\mathrm{d}t^m}\frac{\partial F}{\partial q_i^{(m)}} = 0, \qquad (2)$$

($i = 1, 2, \ldots, n$), which, in general, represent a coupled system of nonlinear, ordinary differential equations (ODEs) of order $2m$. E_i denotes the residual of the ith Euler–Lagrange equation. The $2mn$ constants of integration can be specified by the requirements to satisfy certain boundary conditions. For discrete (point-to-point) movements the boundary conditions are specified at the endpoints of the integration interval:

$$\left.\begin{array}{ll} \mathbf{q}(0) = \mathbf{q}_0, & \mathbf{q}(T) = \mathbf{q}_\mathrm{f} \\ \dot{\mathbf{q}}(0) = \dot{\mathbf{q}}_0, & \dot{\mathbf{q}}(T) = \dot{\mathbf{q}}_\mathrm{f} \\ \vdots & \vdots \\ \mathbf{q}^{(m-1)}(0) = \mathbf{q}_0^{(m-1)}, & \mathbf{q}^{(m-1)}(T) = \mathbf{q}_\mathrm{f}^{(m-1)} \end{array}\right\}. \qquad (3)$$

In the case of rhythmic arm movements of the end-effector, periodic boundary conditions for the generalized velocities and higher derivatives of the form

$$\left.\begin{array}{l} \mathbf{q}(0) = \mathbf{q}_0 \\ \mathbf{q}(T) = \mathbf{q}_\mathrm{f} \\ \dot{\mathbf{q}}(0) = \dot{\mathbf{q}}(T) \\ \vdots \\ \mathbf{q}^{(2m-2)}(0) = \mathbf{q}^{(2m-2)}(T) \end{array}\right\} \qquad (4)$$

can be applied in order to determine the $2mn$ constants.

The existence of a unique solution to the two-point boundary value problem (TPBVP), specified by (2) and (3) or (4), is not guaranteed in general. It depends significantly on the structure of the differential equations and boundary conditions. Under certain conditions, existence and uniqueness proofs can be derived (Keller 1968). Assuming that a solution exists, its determination is, in general, not a trivial task. Several methods, such as shooting or discretization methods, have been developed to solve the TPBVP (Keller 1968).

In this work, it is *assumed* that (i) an optimal trajectory exists and is unique, and (ii) the ith generalized coordinate, $q_i^*(t)$, corresponding to the optimal solution is (at least) a $2m$-time continuously differentiable function in the interval $[0, T]$, where m denotes the order of the highest derivative appearing in the functional (1).

An outline of the suggested algorithm for the numerical solution of the optimization problem is shown in Fig. 1. By expanding the generalized coordinates into a set of basis function the cost functional (1) is transformed into a scalar function of expansion coefficients and is then subjected to a parameter optimization method. The parameter optimization method does not solve the optimization problem with high accuracy but leads to an approximate (suboptimal) solution that can be used as an initial guess for the multiple shooting algorithm. This combination of methods leads to trajectories that satisfy the necessary condition of optimality with high accuracy and thus defines the outcome of the model. Although such a hybrid method was previously developed for optimal control problems of an industrial robot by von Stryk and Schlemmer (1994), it has not been applied to optimization problems that arise in the theory of human motor control. As will be shown in the following section, the parameterization of the generalized coordinates is problem specific and leads to different parameterization schemes depending on the type of boundary conditions being imposed.

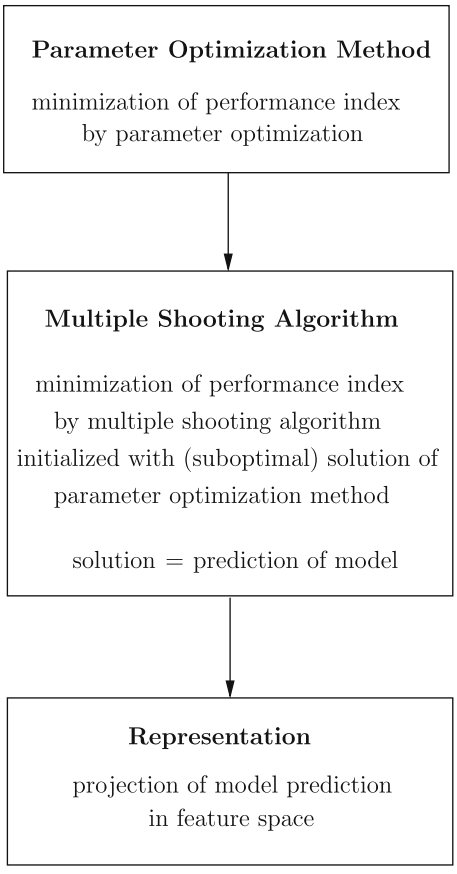

Fig. 1 Hybrid algorithm consisting of a parameter optimization method and a multiple shooting algorithm. The solution of the parameter optimization method is used as an initial guess for the multiple shooting algorithm. The solution of the multiple shooting algorithm defines the prediction of the model and can be projected onto the set of basic functions (feature space) for further analysis

Once the optimal solution is determined using the hybrid method, it can be projected onto the set of basis functions resulting in a discrete representation of the optimal solution in terms of expansion coefficients (feature space) that can be used for further analysis. The parameterization and the shooting algorithm are presented in detail in the following sections.

2.1 Parameterization of generalized coordinates

Each generalized coordinate is parameterized in order to convert the nonlinear cost functional (1) into a nonlinear cost

function of expansion coefficients. The set of functions used in the expansion of the generalized coordinates is chosen to be a complete set of orthogonal functions in the interval $[0, T]$ that satisfy the imposed boundary conditions (3) or (4). The completeness of the set of functions guarantees that any function that is square integrable in the interval $[0, T]$ can be represented uniquely in terms of expansion coefficients (in the mean square limit). Each generalized coordinate can thus be assigned a discrete vector of expansion coefficients. The objective consists of finding a complete set of functions that is compatible with the imposed boundary conditions. The expansion scheme depends therefore on the type of movements. Two types of movements which are of particular interest in motor control research are considered in this work: *discrete* and *rhythmic* movements.

2.1.1 Discrete movements

In the case of discrete point-to-point movements with boundary conditions specified by (3), the generalized coordinates are expanded as

$$q_{i,N}(\tau) = \sum_{k=0}^{2m-1} p_{ik}\tau^k + \sum_{k=0}^{N} c_{ik}\phi_k^{(m)}(\tau), \quad i = 1, \ldots, n, \tag{5}$$

where $\tau = t/T$ is movement time normalized with respect to the total movement duration and N denotes the order of the expansion. In these equations, the ith generalized coordinate is represented by the sum of a polynomial of order $2m-1$ with coefficients p_{ik}, $(k = 0, 1, \ldots, 2m-1)$, corresponding to the number of free parameters per DOF, augmented by a series built of a set of basis functions $\{\phi_k^{(m)}(\tau), k = 0, 1, \ldots\}$ over the normalized time interval [0,1]. The coefficients, p_{ik}, are chosen such that the polynomial satisfies the inhomogeneous boundary condition (3), whereas the series consisting of the set of basis functions satisfies homogeneous boundary conditions for any choice of expansion coefficients.

The explicit expressions for the polynomial coefficients are given in the Appendix A for $m = 1, 2, 3$ and the explicit form of the basis functions is derived in the following.

The basis functions, $\{\phi_k^{(m)}(\tau), k = 0, 1, \ldots\}$, are defined in terms of Jacobi polynomials $P_n^{(\alpha,\beta)}(x)$, which can be represented as

$$P_n^{(\alpha,\beta)}(x) = \frac{1}{2^n}\sum_{k=0}^{n}\binom{n+\alpha}{k}\binom{n+\beta}{n-k}(x-1)^{n-k}(x+1)^k \tag{6}$$

for $x \in [-1, 1]$ and $\alpha, \beta > -1$ (Abramowitz and Stegun 1972). The Jacobi polynomials form a complete set of orthogonal functions in the interval $[-1, 1]$ with respect to the weighting function

$$w(x) = (1-x)^\alpha(1+x)^\beta. \tag{7}$$

Thus

$$\left(P_i^{(\alpha,\beta)}, P_j^{(\alpha,\beta)}\right)_w := \int_{-1}^{1} P_i^{(\alpha,\beta)}(x)w(x)P_j^{(\alpha,\beta)}(x)\mathrm{d}x = \delta_{i,j}h_i^{(\alpha,\beta)} \tag{8}$$

where $\delta_{i,j}$ is the Kronecker-delta and the constant $h_i^{(\alpha,\beta)}$ is given by

$$h_i^{(\alpha,\beta)} = \frac{2^{\alpha+\beta+1}}{2i+\alpha+\beta+1}\frac{\Gamma(i+\alpha+1)\Gamma(i+\beta+1)}{i!\Gamma(i+\alpha+\beta+1)}, \tag{9}$$

with the Gamma function Γ.

The Jacobi polynomials in combination with the weighting function are selected for the description of point-to-point movements since the boundary conditions (3) can be satisfied by the product of the square root of the weighting function and the Jacobi polynomial, evaluated for $\alpha = \beta = 2m$ at the shifted argument $x = 2\tau - 1$. The basis functions appearing in (5) are therefore defined as

$$\phi_k^{(m)}(\tau) = C_{k,m}\sqrt{w(x)}P_k^{(2m,2m)}(x)\big|_{x=2\tau-1} = C_{k,m}2^{2m}\tau^m(1-\tau)^m P_k^{(2m,2m)}(2\tau-1), \tag{10}$$

with a normalization factor

$$C_{k,m} = \frac{1}{\sqrt{h_k^{(2m,2m)}}} \tag{11}$$

and m denotes the order of the highest derivative appearing in the cost functional (1). Wada et al. (2001) proposed the expansion scheme (10) in terms of shifted Jacobi polynomials for $m = 3$ and used it for the numerical computation of the minimum commanded torque change trajectories. In this work, we will use the expansion scheme for different values of $m = 1, 2, 3$ and use it as a novel tool to derive a discrete representation of point-to-point movements.

The basis functions satisfy an orthogonality relation in the interval [0, 1]:

$$\int_0^1 \phi_i^{(m)}(\tau)\phi_j^{(m)}(\tau)\mathrm{d}\tau = \frac{1}{2}\delta_{i,j}. \tag{12}$$

Figure 2 shows the first four basis functions with $m = 3$.

Once the optimal solution, $q_i^*(\tau)$, is determined, the solution can be projected onto the orthogonal basis and thus be represented in terms of expansion coefficients which are given with (5) and (12) as

$$c_{ik} = 2\int_0^1 Q_i^*(\tau)\phi_k^{(m)}(\tau)\mathrm{d}\tau \tag{13}$$

where

$$Q_i^*(\tau) = q_i^*(\tau) - \sum_{k=0}^{2m-1} p_{ik}\tau^k. \tag{14}$$

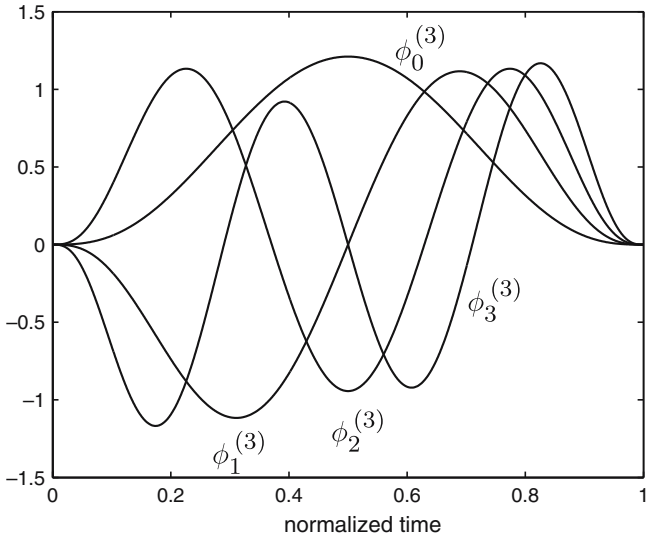

Fig. 2 The first four basis functions of the expansion scheme $m = 3$ used in the description of discrete (point-to-point) movements

2.1.2 Rhythmic movements

In the case of rhythmic movements with periodic boundary conditions of the form (4), Fourier series are selected to approximate the generalized coordinates due to their intrinsic periodicity (Richardson and Flash 2002). Since the function is periodic in its first and all higher derivatives, a Fourier expansion is assumed for the first derivative, i.e.,

$$\dot{q}_{i,N}(t) = \frac{a_{0i}}{2T} + \frac{1}{T}\sum_{k=1}^{N}\left[a_{ik}\cos\left(\frac{2\pi kt}{T}\right) + b_{ik}\sin\left(\frac{2\pi kt}{T}\right)\right], \tag{15}$$

Integration of (15) in the interval $[0, T]$ leads to

$$q_{i,N}(t) = C_i + \frac{a_{0i}t}{2T} + \sum_{k=1}^{N}\left[\frac{a_{ik}}{2\pi k}\sin\left(\frac{2\pi kt}{T}\right) - \frac{b_{ik}}{2\pi k}\cos\left(\frac{2\pi kt}{T}\right)\right]. \tag{16}$$

The constants a_{0i} and C_i are determined such that the boundary conditions (3) are satisfied leading to

$$q_{i,N}(\tau) = q_{i0} + (q_{if} - q_{i0})\tau + \sum_{k=1}^{N}\left[\frac{a_{ik}}{2\pi k}\sin(2\pi k\tau) + \frac{b_{ik}}{2\pi k}(1 - \cos(2\pi k\tau))\right], \tag{17}$$

where $\tau = t/T$ is the normalized time with respect to the period of the movement T. The Fourier coefficients are determined by the well-known expressions

$$a_{ik} = 2\int_0^1 R_i^*(\tau)\cos(2\pi k\tau)\mathrm{d}\tau, \tag{18}$$

$$b_{ik} = 2\int_0^1 R_i^*(\tau)\sin(2\pi k\tau)\mathrm{d}\tau, \tag{19}$$

where, with $\dot{q}_i^*(\tau)$ denoting the first derivative of the optimal solution,

$$R_i^*(\tau) = T\dot{q}_i^*(\tau) - (q_{if} - q_{i0}). \tag{20}$$

Finally it is noted that if periodic boundary conditions are imposed on the generalized coordinates, i.e., $\mathbf{q}(0) = \mathbf{q}(T)$, the polynomial part in the expansion is not required and the coordinates are simply expressed by a Fourier series.

2.1.3 Representation

The parameterization of generalized coordinates leads to a discrete representation of movements. The different boundary conditions for point-to-point and rhythmic movements enforce different expansion schemes for the generalized coordinates resulting in the different representations (13) and (18), (19) for discrete and rhythmic movements, respectively.

A fundamental property of voluntary movements lies in the smoothness of geometrical and kinematic variables that characterize the movement, such as path and speed. The space of expansion coefficients defines, therefore, for real movements a low dimensional feature space, since high frequency contributions are suppressed. It is a well-know fact that the reduction of degrees of freedom is a necessary prerequisite for comparison, recognition and classification of movements.

In this representation, every generalized coordinate, $q_i(\tau)$, can be expressed as a point in the space spanned by the basis functions:

$$\mathbf{u}_i = \begin{cases} (c_{i1}, c_{i2}, c_{i3}, \ldots, c_{iN})^{\mathrm{T}}, & \text{(discrete)} \\ (a_{i1}, b_{i1}, \ldots, a_{iN}, b_{iN})^{\mathrm{T}}, & \text{(rhythmic).} \end{cases} \tag{21}$$

The expansion order, N, can be chosen such that the maximal absolute distance between the generalized coordinate expanded up to order N and the same coordinate expanded up to order $N + 1$ falls below a user-defined threshold. A distance measure, d_{AB}, can be defined between the generalized coordinates, $q_i(\tau)$, resulting from the predictions of two models A and B (or a model A and the experimental data B), as the Euclidean distance in the space of expansion coefficients:

$$d_{\mathrm{AB}} = \sqrt{\left[\mathbf{u}_i^{(\mathrm{A})} - \mathbf{u}_i^{(\mathrm{B})}\right]^2}. \tag{22}$$

The relation (22) defines a metric in the space spanned by the basis functions (feature space) that can be used for comparison of movements. Whether the set of expansion coefficients defines a set of informative features which can be used for recognition and classification of movements or whether informative features can be constructed out of the discrete representation is still an open question and requires further research.

2.2 Parameter optimization method

The functional (1) can be transformed into a scalar function by inserting the expansion of the generalized coordinates, leading to

$$\mathcal{C}(\mathbf{u}_1, \ldots, \mathbf{u}_n) = \int_0^{\mathrm{T}} F\left[\mathbf{q}_N(t), \dot{\mathbf{q}}_N(t), \ldots, \mathbf{q}_N^{(m)}(t), t\right] \mathrm{d}t. \tag{23}$$

Several techniques for the parameter optimization of continuous, nonlinear, unconstrained functions are available. Gradient methods like nonlinear conjugate gradient (CG) and Newton methods, namely Quasi-Newton (QN) and truncated Newton (TN) schemes, are effective methods for finding a local minimum of a multivariate function. They have been studied extensively and an overview of the methods can be found in textbooks (Fletcher 2000; Nocedal and Wright 1999). Several software packages for optimization (e.g., NAG, MATLAB) are available. In this work, a parameter optimization method based on a QN method as implemented in MATLAB is applied.

The minimization of the cost function (23) is accomplished by successively applying a parameter optimization while increasing the expansion order N. The initial guess for the expansion coefficients $\mathbf{u}_i^{(0)}$, $(i = 1, \ldots, n)$ with expansion order $N = 1$ consists of small random perturbations around zero (one coefficient per DOF for discrete movements and two per DOF for rhythmic movements). This provides a set of optimal coefficients for expansion order $N = 1$ which are used as an initial guess (with the other unknown coefficients initialized to zero) for the expansion order with $N = 2$. This iteration scheme is applied successively until convergence is obtained for expansion order $N = N_{\max}$ with expansion coefficients $\tilde{\mathbf{u}}_1, \ldots, \tilde{\mathbf{u}}_n$.

The expansion of the generalized coordinates in terms of the expansion coefficients, $\tilde{\mathbf{u}}_1, \ldots, \tilde{\mathbf{u}}_n$, defines the solution of the parameter optimization method, denoted by $\tilde{\mathbf{q}}(t)$. Higher derivatives of order k, $\tilde{\mathbf{q}}^{(k)}(t)$, follow then by k-times term-by-term differentiation of the series $\tilde{\mathbf{q}}(t)$. The iterative determination of the optimal expansion coefficients works well in all presented examples, as shown later. However, based on extensive simulation studies using different parameter optimization algorithms, it was found that the solution obtained from the parameter optimization method does not satisfy the Euler–Lagrange equation with high accuracy and only provides an approximate solution of the TPBVP.

2.3 Shooting methods

Shooting algorithms are another widely used technique to solve a TPBVP. For the application of a shooting algorithm the Euler-Lagrange equations, (2), are first written as an explicit linear n dimensional system of ODEs of order $2m$,

$$\mathbf{q}^{(2m)}(t) = \mathbf{f}(t, \mathbf{q}(t), \mathbf{q}'(t), \ldots, \mathbf{q}^{(2m-1)}(t)), \tag{24}$$

where it was assumed that the Lagrangian F in Eq. (1) is quadratic in its highest derivative.

For a numerical solution, (24) is further transformed into a first-order system of ODEs of dimension $D = 2mn$ by defining the $2m$ n-dimensional vectors $\mathbf{y}_1(t) = \mathbf{q}(t)$, $\mathbf{y}_2(t) = \dot{\mathbf{q}}(t), \ldots, \mathbf{y}_{2m}(t) = \mathbf{q}^{(2m-1)}(t)$ resulting in

$$\left.\begin{aligned} \mathbf{y}_1' &= \mathbf{y}_2 \\ \mathbf{y}_2' &= \mathbf{y}_3 \\ &\vdots \\ \mathbf{y}_{2m-1}' &= \mathbf{y}_{2m} \\ \mathbf{y}_{2m}' &= \mathbf{f}(t, \mathbf{y}_1, \mathbf{y}_2, \ldots, \mathbf{y}_{2m}) \end{aligned}\right\}. \tag{25}$$

Introducing the D dimensional vectors

$$\mathbf{Y} = \begin{bmatrix} \mathbf{y}_1 \\ \mathbf{y}_2 \\ \vdots \\ \mathbf{y}_{2m} \end{bmatrix}, \quad \mathbf{G} = \begin{bmatrix} \mathbf{y}_2 \\ \vdots \\ \mathbf{y}_{2m} \\ \mathbf{f} \end{bmatrix}, \tag{26}$$

leads to the form of the Euler–Lagrange equations used in the shooting algorithm

$$\mathbf{Y}'(t) = \mathbf{G}(t, \mathbf{Y}(t)). \tag{27}$$

(The transformation of the Euler–Lagrange equation, (2), into the system (27) can be easily performed by using a symbolic mathematics software package such as MATHEMATICA or MAPLE.)

The D boundary conditions for discrete and rhythmic movements can be written in the general form as

$$\mathbf{R}(\mathbf{Y}(0), \mathbf{Y}(T)) = 0, \tag{28}$$

where $\mathbf{R}$ consists of $2m$ vector functions $\mathbf{r}_i$, $i = 1, \ldots, 2m$, of dimension n, i.e.,

$$\mathbf{R} = \begin{bmatrix} \mathbf{r}_1 \\ \mathbf{r}_2 \\ \vdots \\ \mathbf{r}_{2m} \end{bmatrix}. \tag{29}$$

In the case of discrete movements it is

$$\mathbf{r}_i = \mathbf{Y}_i(0) - \mathbf{a}_i, \quad i = 1, \ldots, m, \tag{30}$$

$$\mathbf{r}_{i+m} = \mathbf{Y}_i(T) - \mathbf{b}_i, \quad i = 1, \ldots, m, \tag{31}$$

with

$$\mathbf{a} = \begin{bmatrix} \mathbf{q}_0 \\ \dot{\mathbf{q}}_0 \\ \vdots \\ \mathbf{q}_0^{(m-1)} \end{bmatrix}, \quad \mathbf{b} = \begin{bmatrix} \mathbf{q}_\mathrm{f} \\ \dot{\mathbf{q}}_\mathrm{f} \\ \vdots \\ \mathbf{q}_\mathrm{f}^{(m-1)} \end{bmatrix}, \tag{32}$$

whereas for rhythmic movements

$$\mathbf{r}_1 = \mathbf{Y}_1(0) - \mathbf{q}_0, \tag{33}$$

$$\mathbf{r}_2 = \mathbf{Y}_1(T) - \mathbf{q}_\mathrm{f}, \tag{34}$$

$$\mathbf{r}_{i+2} = \mathbf{Y}_{i+1}(T) - \mathbf{Y}_{i+1}(0), \quad i = 1, \ldots, 2m-2. \tag{35}$$

In a single shooting algorithm the TPBVP is solved by finding a solution of the initial value problem of the form

$$\mathbf{Y}'(t) = \mathbf{G}(t, \mathbf{Y}(t)) \tag{36}$$

with initial condition

$$\mathbf{Y}(0) = \mathbf{s} \tag{37}$$

where the vector $\mathbf{s}$ is a D dimensional starting vector. If $\mathbf{Y} = \mathbf{Y}(t; \mathbf{s})$ denotes the solution of the initial value problem, (36) and (37), the TPBVP is solved if it is possible to find a set of D parameters $\mathbf{s}^*$ such that the boundary conditions are satisfied, i.e.,

$$\mathbf{R}(\mathbf{Y}(0, \mathbf{s}^*), \mathbf{Y}(T, \mathbf{s}^*)) \equiv \mathbf{R}(\mathbf{s}^*, \mathbf{Y}(T, \mathbf{s}^*)) = 0. \tag{38}$$

This is equivalent to finding the roots of a system of D nonlinear equations

$$\mathbf{H}(\mathbf{s}) = 0 \quad \text{with} \quad \mathbf{H}(\mathbf{s}) = \mathbf{R}\left(\mathbf{s}, \mathbf{Y}(T, \mathbf{s})\right), \tag{39}$$

which can be solved iteratively using a Newton method (Fig. 3).

Two main difficulties appear in using single shooting methods. First, the Newton method only converges if an appropriate initial guess for the missing parameters is provided. Second, the achievable accuracy of the solution in a single shooting method grows exponentially with the length of the integration interval (Keller 1968).

The latter can be improved in a multiple shooting algorithm by dividing the integration interval into several subintervals,

$$0 = t_0 < t_1 < \cdots < t_p = T, \tag{40}$$

and applying a single shooting method in each subinterval separately (Stoer and Bulirsch 1980). Multiple shooting algorithms are thus much more robust than single shooting methods. The improved robustness of a multiple shooting algorithm results in an increased complexity since the solution, pieced together by the partial solutions in each subintervals, must not only satisfy the boundary conditions but also be continuous at the partition points. The main parts of the multiple shooting algorithm are summarized briefly. Further details can be found in Stoer and Bulirsch (1980).

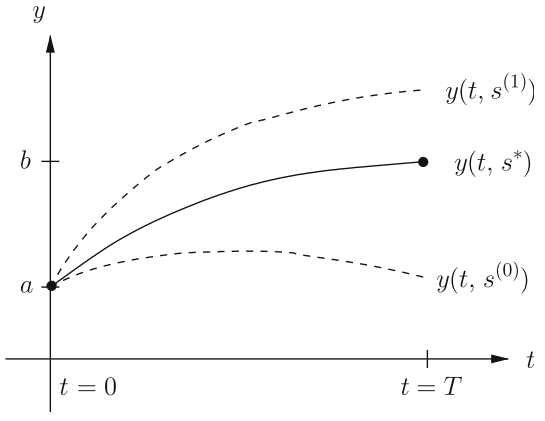

Fig. 3 *Single* shooting algorithm for the solution of a two-point boundary value problem (TPBVP) of the form $y'' = f(t, y, y')$ with boundary conditions $y(0) = a$ and $y(T) = b$. The transformation to a first order system is obtained by setting $y_1 = y$ and $y_2 = y'$ resulting in $\mathbf{Y} = (y_1, y_2)^{\mathrm{T}}$ and $G = (y_2, f(t, y_1, y_2))^{\mathrm{T}}$. The solution is determined by solving the corresponding initial value problem with the initial condition $\mathbf{Y} = (s_1, s_2)^{\mathrm{T}}$. The unknown parameters (s_1, s_2) are determined by the $D = 2$ boundary conditions $\mathbf{H}(s_1, s_2) = (y_1(0, s_1) - a, y_1(T, s_2) - b)^{\mathrm{T}} \equiv (s_1 - a, y_1(T, s_2) - b)^{\mathrm{T}} = 0$, which can be solved iteratively using a Newton method. The parameter $s = s_2$ corresponds in this example to the slope of the trajectory at the starting point. The solution, $y = y(t, s^*)$, and trajectories corresponding to two iterations of the parameter s are shown

Let $\mathbf{Y}(t; t_k, \mathbf{s}_k)$ be the solution of the initial value problem $\mathbf{Y}' = \mathbf{G}(t, \mathbf{Y})$ with $\mathbf{Y}(t_k) = \mathbf{s}_k$ in the interval $[t_k, t_{k+1})$, where $k = 0, 1, \ldots, p-1$. The problem now consists of the computation of $p+1$ vectors $\mathbf{s}_k$, $k = 0, 1, \ldots, p$, of dimension D in such a way that the piecewise defined function

$$\mathbf{Y}(t) := \mathbf{Y}(t; t_k, \mathbf{s}_k), \quad \text{for} \quad t \in [t_k, t_{k+1}) \tag{41}$$

$$\mathbf{Y}(T) := \mathbf{s}_p \tag{42}$$

is continuous and satisfies the boundary conditions $\mathbf{R}(\mathbf{Y}(0), \mathbf{Y}(T)) = 0$. This leads to the following conditions

$$\mathbf{Y}(t_{k+1}; t_k, \mathbf{s}_k) = \mathbf{s}_{k+1}, \quad k = 0, 1, \ldots, p-1, \tag{43}$$

$$\mathbf{R}(\mathbf{s}_0, \mathbf{s}_p) = 0. \tag{44}$$

These conditions are equivalent to solving the system of $D(p+1)$ equations

$$\mathbf{H}(\mathbf{s}_0, \mathbf{s}_1, \ldots, \mathbf{s}_p) = \begin{bmatrix} \mathbf{Y}(t_1; t_0, \mathbf{s}_0) - \mathbf{s}_1 \\ \mathbf{Y}(t_2; t_1, \mathbf{s}_1) - \mathbf{s}_2 \\ \vdots \\ \mathbf{Y}(t_p; t_{p-1}, \mathbf{s}_{p-1}) - \mathbf{s}_p \\ \mathbf{R}(\mathbf{s}_0, \mathbf{s}_p) \end{bmatrix} = 0 \tag{45}$$

for the $D(p+1)$ unknowns $\mathbf{s}_0, \mathbf{s}_1, \ldots, \mathbf{s}_p$ which can be computed iteratively using a Newton method (Fig. 4). The initial guess for the iterative solution, $(\mathbf{s}_0^{(0)}, \mathbf{s}_1^{(0)}, \ldots, \mathbf{s}_p^{(0)})$, of system (45) is provided by the solution of the parameter optimization method, i.e., it is set to

$$\mathbf{s}_k^{(0)} = \begin{bmatrix} \tilde{\mathbf{q}}(t_k) \\ \dot{\tilde{\mathbf{q}}}(t_k) \\ \vdots \\ \tilde{\mathbf{q}}^{(2m-1)}(t_k) \end{bmatrix}, \quad k = 0, 1, \ldots, p. \tag{46}$$

The outcome of the multiple shooting algorithm initialized with the solution of the parameter optimization method gives the optimal solution, which defines the predictions of the model. The solution can be projected onto the basis functions (feature space), as described in Sect. 2.1, leading to a discrete representation in terms of expansion coefficients, $\mathbf{u}_i^*$, $i = 1, \ldots, n$.

In this work, a multiple shooting algorithm in the form of the software package MUMUS (*Mu*nich *Mu*ltiple *S*hooting) with $p = 100$ subintervals is used. Further details about the MUMUS algorithm and the actual implementation are available in the documentation (Bulirsch 1971).

In the following sections, results from simulations of human arm movements based on the minimization of different nonlinear performance indices are presented and the robustness of the suggested computational method is demonstrated. Models of planar point-to-point movements involving nonlinear costs are considered first, followed by models of planar

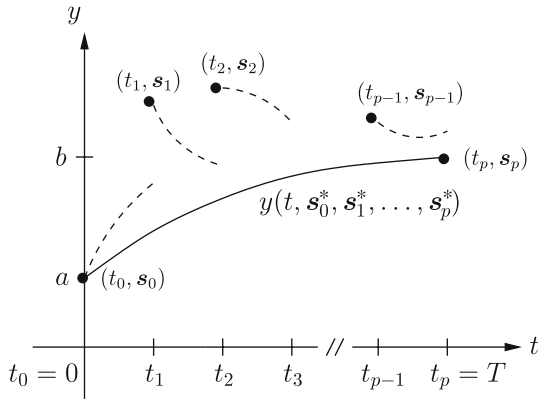

Fig. 4 *Multiple* shooting algorithm for the solution of a TPBVP of the form $y'' = f(t, y, y')$ with boundary conditions $y(0) = a$ and $y(T) = b$. The transformation to a first-order system is performed as in the single shooting method. For the numerical solution the integration interval is first divided into p subintervals $0 = t_0 < t_1 < \cdots < t_p = T$. The solution is determined by solving the initial value problem in each subinterval with the initial condition $\mathbf{Y}(t_k) = \mathbf{s}_k, k = 0, 1 \ldots, p-1$, where the vector $\mathbf{s}_k = (s_{k,1}, s_{k,2})^{\mathrm{T}}$ consists of $D = 2$ components. The $D(p+1)$ unknown parameters, $\mathbf{s}_0, \mathbf{s}_1, \ldots, \mathbf{s}_p$, are determined by the boundary conditions and the continuity conditions at the partition points. The solution of the TPBVP, $y = y(t, \mathbf{s}_0^*, \mathbf{s}_1^*, \ldots, \mathbf{s}_p^*)$, is determined iteratively using a Newton method. A set of partial solutions of the initial value problem in each subinterval is shown (*dashed lines*) resulting from one iteration of the Newton method

rhythmic movements derived from a nonlinear optimization criterion. Finally, point-to-point movements of a four DOF arm in three-dimensional space are analyzed assuming that the paths follow geodesics in configuration space.

The first problems within the class of planar point-to-point movements are defined by ones treated with respect to the one-parameter family of mean-squared derivative (MSD) costs of the end-effector. They define a set of test problems with known analytical solutions, whereas for all the other presented examples no analytical results are available.

The test problems which include the minimum-jerk model (Flash and Hogan 1985) are analyzed in joint-angular space where the cost function is nonlinear. The minimum commanded torque change model (Nakano et al. 1999; Wada et al. 2001; Kaneko et al. 2005), as the dynamical analog to the kinematic minimum-jerk model, is considered next. The latter does not have an analytical solution and thus provides a challenging test to the method. Moreover, the simulation results are analyzed in the low dimensional feature space of expansion coefficients. This allows, for example, a quantitative comparison of the hand paths derived from different optimization criteria.

Rhythmic movements in the form of repeatedly tracing a given path in the form of an ellipse or a cloverleaf are considered in the following. The derived speed-curvature relations are of special interest due to the implications they have in relation to motor segmentation. It will be shown that these movements have a low dimensional representation in Fourier space.

The optimization method can also be applied to movements in three-dimensional space as demonstrated in the last simulation example, where the geodesics of a four DOF arm in configuration space with respect to a metric defined by the manipulator inertia matrix are computed.

2.4 Test problems

In the test problems, point-to-point movements of the end-effector of a two DOF planar arm with upper arm length l_1 and forearm length l_2 are analyzed (Fig. 5). The performance index is taken from the one parameter family of MSD costs defined by the squared mth-derivative of the end-effector position vector $\mathbf{x} = (x, y)^{\mathrm{T}}$ integrated over the movement time (Harris 1998; Richardson and Flash 2002):

$$C_m = \int_0^{\mathrm{T}} \left[\left(\frac{d^m \mathbf{x}}{dt^m} \right)^{\mathrm{T}} \cdot \left(\frac{d^m \mathbf{x}}{dt^m} \right) \right] \mathrm{d}t, \tag{47}$$

$(m = 1, 2, \ldots)$, subject to the boundary conditions

$$\left.\begin{array}{ll} \mathbf{x}(0) = \mathbf{x}_0, & \mathbf{x}(T) = \mathbf{x}_{\mathrm{f}}, \\ \dot{\mathbf{x}}(0) = 0, & \dot{\mathbf{x}}(T) = 0, \\ \vdots & \vdots \\ \mathbf{x}^{(m-1)}(0) = 0, & \mathbf{x}^{(m-1)}(T) = 0, \end{array}\right\} \tag{48}$$

where the total movement time is T and $\mathbf{x}_0$ and $\mathbf{x}_{\mathrm{f}}$ denote the initial and final hand location, respectively.

This family of cost functionals consists of inner products of derivatives of the hand vector and thus defines a measure of smoothness. Experimental findings by Flash and Hogan (1985) suggest that minimal mean-squared jerk trajectories ($m = 3$) provide a suitable description of planar point-to point human arm movements. This is not the case for minimal

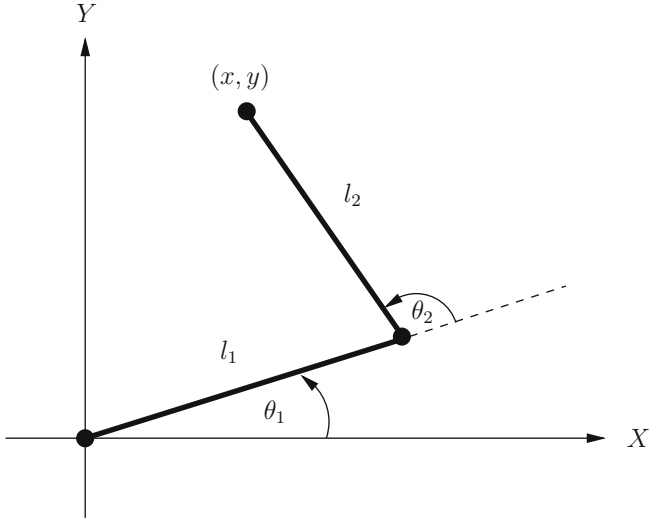

Fig. 5 Planar two degree-of-freedom (DOF) manipulator used to study the minimum-jerk model (MJ) and the minimum commanded torque change model (MCTC)

mean-squared velocity ($m = 1$) and minimal mean-squared acceleration ($m = 2$), whereas the predictions of the minimal mean-squared change of rate of jerk ($m = 4$), sometimes called snap, also provide a reasonable fit to the experimental data.

The problem of minimizing (47) subject to the boundary conditions of (48) can be solved analytically (Richardson and Flash 2002). The optimal solution has the form

$$\mathbf{x}^*(t) = \mathbf{x}_0 + f_m(\tau)(\mathbf{x}_\mathrm{f} - \mathbf{x}_0), \tag{49}$$

where $\tau = t/T$ is the normalized time and

$$f_m(\tau) = \frac{(2m-1)!\tau^m}{(m-1)!^2 m} {}_2F_1(m; 1-m; 1+m; \tau), \tag{50}$$

with the generalized hypergeometric function ${}_2F_1$. In particular, for $m = 1, 2, 3$:

$$f_1(\tau) = \tau, \tag{51}$$

$$f_2(\tau) = -2\tau^3 + 3\tau^2, \tag{52}$$

$$f_3(\tau) = 6\tau^5 - 15\tau^4 + 10\tau^3. \tag{53}$$

Since an analytical solution is available, it can be used for comparison to the predictions of the method. In order to make the computational problem more challenging the comparison is performed in configuration space. It involves first transforming the optimization problem, (47), (48), into joint angle space, $\boldsymbol{\theta} = (\theta_1, \theta_2)^\mathrm{T}$, where the cost is a nonlinear function and therefore serves as a challenging test of the method. The results are compared to the known Cartesian solution projected into joint space. It should be noted that the projected solution is a solution of the corresponding variational problem formulated in joint space due to the invariance of the Euler-Lagrange equation under coordinate transformation.

The projection of the cost (47) into joint-space is given by the forward kinematic equations, yielding

$$x = l_1 \cos(\theta_1) + l_2 \cos(\theta_1 + \theta_2), \tag{54}$$

$$y = l_1 \sin(\theta_1) + l_2 \sin(\theta_1 + \theta_2). \tag{55}$$

The inverse kinematic relations can be written as

$$\theta_1 = \arctan2(y, x) - \arccos\left(\frac{r^2 + l_1^2 - l_2^2}{2l_1 r}\right), \tag{56}$$

$$\theta_2 = \pi - \arccos\left(\frac{l_1^2 + l_2^2 - r^2}{2l_1 l_2}\right) \tag{57}$$

with $r = \sqrt{x^2 + y^2}$ and $\arctan2(y, x) = \arctan(y/x) + \mathrm{sign}(y)(1 - \mathrm{sign}(x))\pi/2$. The optimal solution in joint space, $\boldsymbol{\theta}^*(\tau) = (\theta_1^*(\tau), \theta_2^*(\tau))^\mathrm{T}$, follows then by inserting (49) into (56) and (57).

For the numerical solution of the optimization problem the joint angles are first expanded according to (5) and inserted into the cost function. A QN method is used for the parameter optimization (e.g., as implemented in MATLAB). The boundary conditions were set to $\boldsymbol{\theta}_0 = (0, \pi/6)^\mathrm{T}$rad, $\boldsymbol{\theta}_\mathrm{f} = (2\pi/3, \pi/3)^\mathrm{T}$ rad and the total movement duration was chosen to be $T = 1$ s. The arm length of the upper and forearm were set to $l_1 = 0.30$ m and $l_1 = 0.32$ m, respectively.

A measure of how close the necessary condition of optimality is satisfied is derived from the residual of the Euler–Lagrange equation defined in (2). This error is defined by the maximum value of the sum of absolute residuals (Wada et al. 2001), i.e.,

$$E_\mathrm{max} = \max_{0 \le t \le T} \sum_{i=1}^{2} |E_i(t)|. \tag{58}$$

If the solution for the trajectory leads to an error $E_\mathrm{max} = 0$ the trajectory satisfies the Euler–Lagrange equations and thus the necessary conditions of optimality are fulfilled.

Table 1 shows the results of the parameter optimization method applied to the MSD cost for $m = 1, 2, 3$. Although the optimal value of the cost was recovered well in all test problems, there remains a large error of the Euler–Lagrange equation using the parameter optimization method. This is related to the fact the higher derivatives converge slowly (if at all) to the optimal solution, in particular, at the boundaries. Figure 6 shows the comparison of (a) the exact optimal joint angular positions, (b) accelerations and (c) the fourth derivatives of joint angular positions of the minimum-jerk model with the results obtained using a parameter optimization method. Whereas the joint angular positions and joint angular accelerations are recovered reasonably well, large deviations occur for the joint angular snaps, in particular at the boundaries, resulting in a large residual of the Euler–Lagrange equations (Table 1).

The error resulting from the multiple shooting algorithm is several order smaller than the error obtained with the parameter optimization method. The solution obtained by the parameter optimization method is thus not optimal.

A method which worked well in practice consisted of combining the parameter optimization method with a multiple shooting algorithm. The solution of the parameterization method was used as an initial guess for the multiple shooting algorithm. In this way the residual of the Euler–Lagrange equations was significantly reduced and the necessary condition of optimality was satisfied with high accuracy.

The results of the multiple shooting algorithm initialized with the solution of the parameter optimization method are shown in Table 1. Figure 7 shows the difference in joint trajectories, $\Delta\theta_i(\tau) = \theta_i(\tau) - \theta_i^*(\tau)$, $i = 1, 2$, between the analytical and the numerical solution computed with the hybrid method for all three test problems $m = 1, 2, 3$. The optimal

Table 1 Results of the parameter optimization method and the multiple shooting algorithm for the mean-squared derivative costs with $m = 1, 2, 3$

Exact	Parameter optimization			Multiple shooting		
m	$\mathcal{C}^*$	N	$\mathcal{C}$	E_max	$\mathcal{C}$	E_max
1	1.1064	20	1.1064	2.3e + 0	1.10644	6.3e − 14
2	13.2773	40	13.2773	4.2e + 5	13.2773	3.8e − 12
3	796.646	50	804.572	1.5e + 10	796.646	1.5e − 8

The exact value of the cost is given by $\mathcal{C}^*$. N is the expansion order used in the parameter optimization and $\mathcal{C}$ is the numerically obtained value for the minimal cost

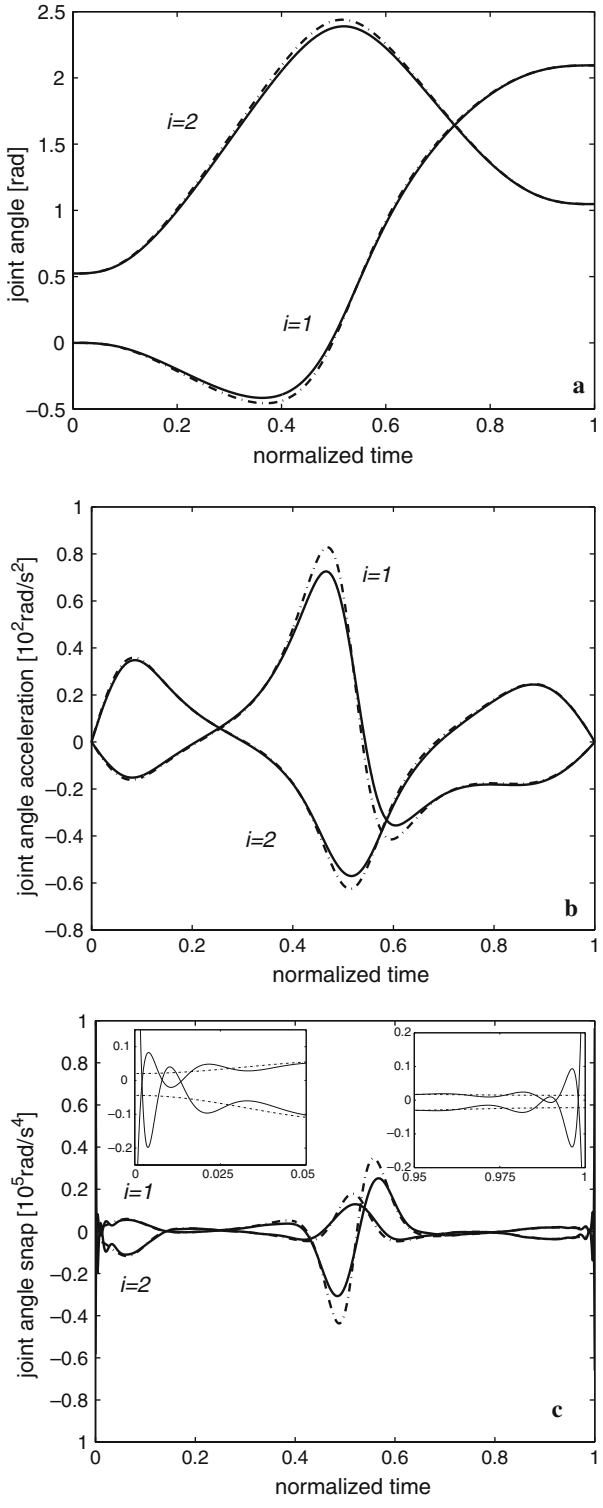

Fig. 6 Comparison of the exact optimal joint **a** angular positions, **b** accelerations, **c** snaps of the MJ (*dash-dotted*) for the two DOF ($i = 1, 2$) and the approximate results derived from the minimization of the cost function using the parameter optimization method (*solid*). Large deviations from the exact solution occur for the joint angular snaps, in particular near the boundaries which are magnified in the inserts. Simulation parameters: $\boldsymbol{\theta}_0 = (0, \pi/6)^{\mathrm{T}}$ rad, $\boldsymbol{\theta}_{\mathrm{f}} = (2\pi/3, \pi/3)^{\mathrm{T}}$ rad, $T = 1\,\mathrm{s}$, $l_1 = 0.30\,\mathrm{m}$ and $l_2 = 0.32\,\mathrm{m}$

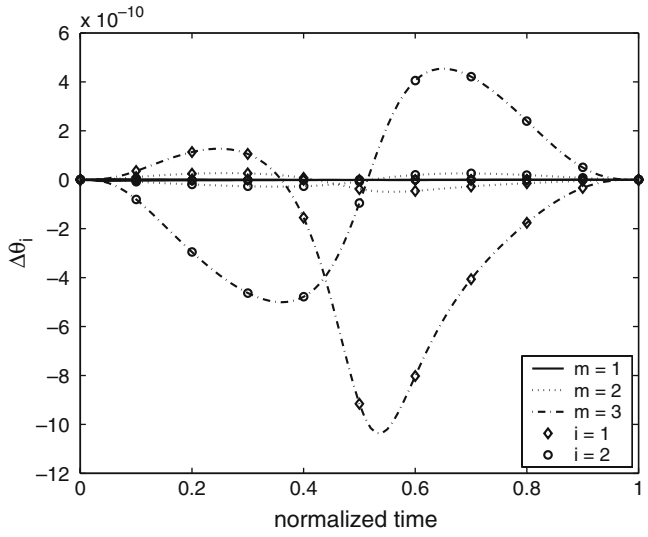

Fig. 7 Errors in joint trajectories, $\Delta\theta_i(\tau) = \theta_i(\tau) - \theta_i^*(\tau)$, $i = 1, 2$, between the analytical and numerical solutions computed with the hybrid method for all three test problems $m = 1, 2, 3$, where m denotes the highest derivative appearing in the cost functional

solution can be recovered with high accuracy as shown by the small error, $|\Delta\theta_i(\tau)| < 10\mathrm{e}-9$, $i = 1, 2$.

Once the optimal solution is determined it can be represented in terms of basis functions. For example, the optimal joint angular trajectories for the MSD cost with $m = 3$, computed above, have the following representation (up to expansion order $N = 10$):

$$\mathbf{u}^*_{\theta_1} = \big[-0.7625, 0.2475, 0.0494, -0.0648, -0.0309, 0.0300, 0.0164, -0.0146, -0.0084, 0.0070, 0.0049\big],$$

$$\mathbf{u}^*_{\theta_2} = \big[1.3017, -0.0457, -0.0309, -0.0211, 0.0253, 0.0046, -0.0119, -0.0017, 0.0043, 0.0016, -0.0022\big].$$

As expected, the magnitude of the expansion coefficients is decreasing with increasing expansion order.

2.5 Minimum commanded torque change model

The minimum torque change model (Uno et al. 1989) and the minimum commanded torque change model (Nakano et al. 1999; Wada et al. 2001; Kaneko et al. 2005) applied to movements in a horizontal or vertical plane can be considered as the dynamic analog to the kinematic minimum-jerk model. The cost function for the minimum commanded torque change model is defined by

$$\mathcal{C} = \int_0^{\mathrm{T}} \left(\frac{\mathrm{d}\boldsymbol{\tau}}{\mathrm{d}t}\right)^{\mathrm{T}} \left(\frac{\mathrm{d}\boldsymbol{\tau}}{\mathrm{d}t}\right) \mathrm{d}t, \tag{59}$$

where the torques, $\boldsymbol{\tau} = (\tau_1, \tau_2)^{\mathrm{T}}$, around the shoulder and the elbow are specified by

$$\boldsymbol{\tau} = M(\boldsymbol{\theta})\ddot{\boldsymbol{\theta}} + C(\boldsymbol{\theta}, \dot{\boldsymbol{\theta}})\dot{\boldsymbol{\theta}} + B\dot{\boldsymbol{\theta}} + \mathbf{N}(\boldsymbol{\theta}) \tag{60}$$

and the joint angular vector is defined as for the minimum-jerk model.

The manipulator inertia matrix M, the Coriolis and centrifugal matrix C, the viscosity matrix B and the gravitational torques $\mathbf{N}$ are given by

$$M(\boldsymbol{\theta}) = \begin{bmatrix} \alpha + 2\beta\cos\theta_2 & \delta + \beta\cos\theta_2 \\ \delta + \beta\cos\theta_2 & \delta \end{bmatrix}, \tag{61}$$

$$C(\boldsymbol{\theta}, \dot{\boldsymbol{\theta}}) = \begin{bmatrix} -\beta\dot{\theta}_2\sin\theta_2 & -\beta(\dot{\theta}_1 + \dot{\theta}_2)\sin\theta_2 \\ \beta\dot{\theta}_1\sin\theta_2 & 0 \end{bmatrix}, \tag{62}$$

$$\mathbf{N}(\boldsymbol{\theta}) = g \begin{bmatrix} \gamma\cos\theta_1 + \rho\cos(\theta_1 + \theta_2) \\ \rho\cos(\theta_1 + \theta_2) \end{bmatrix}, \tag{63}$$

$$B = \begin{bmatrix} b_{11} & b_{12} \\ b_{12} & b_{22} \end{bmatrix} \tag{64}$$

with the constants

$$\alpha = I_1 + I_2 + m_1 r_1^2 + m_2(l_1^2 + r_2^2) \tag{65}$$

$$\beta = m_2 l_1 r_2 \tag{66}$$

$$\delta = I_2 + m_2 r_2^2 \tag{67}$$

$$\gamma = m_1 r_1 + m_2 l_1 \tag{68}$$

$$\rho = m_2 r_2 \tag{69}$$

and the experimentally determined numerical constants of the viscosity matrix b_{11}, b_{12}, b_{22}. For movements in the horizontal plane, where the gravitational torque vanishes, the cost is denoted with $\mathcal{C}_\mathrm{h}$, whereas for movements in the vertical plane the cost is $\mathcal{C}_\mathrm{v}$.

The physical parameters used in the simulation are shown in Table 2 and the numerical values of the components of the viscosity matrix for movements in the horizontal plane are given by

$$B_\mathrm{h} = \begin{bmatrix} 0.74 & 0.10 \\ 0.10 & 0.82 \end{bmatrix} (\mathrm{kg\,m^2/s}), \tag{70}$$

whereas for movements in the vertical plane

$$B_\mathrm{v} = \begin{bmatrix} 0.90 & 0.27 \\ 0.27 & 1.0 \end{bmatrix} (\mathrm{kg\,m^2/s}). \tag{71}$$

(Nakano et al. 1999).

The optimal solution for the joint angular trajectories is determined by first expanding the joint angles, $\boldsymbol{\theta} = (\theta_1, \theta_2)^\mathrm{T}$, according to expansion scheme (5) with $m = 3$. Inserting these expansions into the cost function (59) followed by a parameter optimization leads to the initial guess for the multiple shooting method. The results of the parameter optimization method and the multiple shooting algorithm are shown in Table 3 for movements between a set of targets $\mathbf{T}_1, \ldots, \mathbf{T}_6$ within a horizontal plane and for movements within a vertical plane against the direction of the gravitational field. The hand paths are shown in Fig. 8 for the (a) horizontal and (b) vertical condition. The shoulder joint is located at the position (0, 0).

Table 2 Parameters for the arm model used in the simulation of the minimum commanded torque change (MCTC) model (Nakano et al. 1999)

Parameter	Shoulder joint ($i = 1$)	Elbow joint ($i = 2$)
Mass: m_i (kg)	1.50	1.11
Length: l_i (m)	0.345	0.30
Distance to center of mass: r_i (m)	0.11	0.17
Moment of inertia: I_i ($\mathrm{kg\,m^2}$)	0.029	0.047

Table 3 Results of optimization for the minimum commanded torque change model describing movements in the *horizontal* and *vertical* plane between different targets in the workspace (in m)

Targets	Parameter optimization			Multiple shooting	
$\mathbf{x}_0 \to \mathbf{x}_\mathrm{f}$	N	$\mathcal{C}_\mathrm{h}$	E_max	$\mathcal{C}_\mathrm{h}$	E_max
$\mathbf{T}_1 \to \mathbf{T}_2$	15	22.223	1.9e + 4	22.416	3.4e − 10
$\mathbf{T}_1 \to \mathbf{T}_4$	15	35.327	2.5e + 4	35.791	9.2e − 10
$\mathbf{T}_1 \to \mathbf{T}_6$	15	31.119	6.4e + 4	31.311	1.8e − 10
$\mathbf{T}_3 \to \mathbf{T}_6$	15	68.824	1.3e + 5	68.950	9.7e − 11
$\mathbf{T}_5 \to \mathbf{T}_4$	15	65.337	1.2e + 5	65.963	1.5e − 9
$\mathbf{x}_0 \to \mathbf{x}_\mathrm{f}$	N	$\mathcal{C}_\mathrm{v}$	E_max	$\mathcal{C}_\mathrm{v}$	E_max
$\mathbf{T}_1 \to \mathbf{T}_2$	15	36.419	1.8e + 4	36.637	9.1e − 10
$\mathbf{T}_1 \to \mathbf{T}_4$	15	59.368	2.8e + 4	60.179	3.6e − 9
$\mathbf{T}_1 \to \mathbf{T}_6$	15	70.291	9.3e + 4	70.383	4.2e − 10
$\mathbf{T}_3 \to \mathbf{T}_6$	15	167.457	1.7e + 5	167.527	2.2e − 10
$\mathbf{T}_5 \to \mathbf{T}_4$	15	132.303	8.5e + 4	134.025	4.8e − 9

$\mathbf{T}_1 = (0, 0.3)^\mathrm{T}$, $\mathbf{T}_2 = (0, 0.6)^\mathrm{T}$, $\mathbf{T}_3 = (0.2, 0.4)^\mathrm{T}$, $\mathbf{T}_4 = (0.2, 0.6)^\mathrm{T}$, $\mathbf{T}_5 = (-0.2, 0.35)^\mathrm{T}$, $\mathbf{T}_6 = (-0.2, 0.55)^\mathrm{T}$

The difference in hand paths resulting from the minimum commanded torque change model and the minimum-jerk model is analyzed in the space of expansion coefficients. It should be noted that the suggested expansion scheme is not only applicable for the trajectories but also for the geometric hand path in the workspace. A hand path, given by $y = y(x)$, with boundary conditions specified by $y(x_0) = y_0$ and $y(x_\mathrm{f}) = y_\mathrm{f}$, can be analyzed using an expansion scheme of the form (10) with $m = 1$ when expressing the path in terms of a nondimensional parameter $\lambda = (x - x_0)/(x_\mathrm{f} - x_0) \in [0, 1]$[1]. The expansion for the hand path is then given by

$$\tilde{y}(\lambda) = y_0 + (y_\mathrm{f} - y_0)\lambda + \sum_{k=0}^{N} c_k \phi_k^{(1)}(\lambda). \tag{72}$$

Relation (72) implies that minimum-jerk hand paths, defined by straight lines in the workspace, are represented as the null-vector in the space of expansion coefficients. The distance between two hand paths resulting from two models A and B is, following (22), defined by

$$d_\mathrm{AB} = \sqrt{\sum_{k=0}^{N} \left[c_k^{(\mathrm{A})} - c_k^{(\mathrm{B})}\right]^2} \tag{73}$$

with a user-defined expansion order N.

Table 4 shows the results for the distances of hand paths in expansion coefficient space between the minimum-jerk model (MJ) and the minimum commanded torque change model in the horizontal plane (MCTC(h)). The right column shows the distances between the hand paths derived from the minimum commanded torque change model in the horizontal and the vertical condition (MCTC(v)). No significant influence of the gravitational torque on the hand paths is observed.

[1] If $x_0 = x_\mathrm{f}$, the x and y axes can be interchanged.

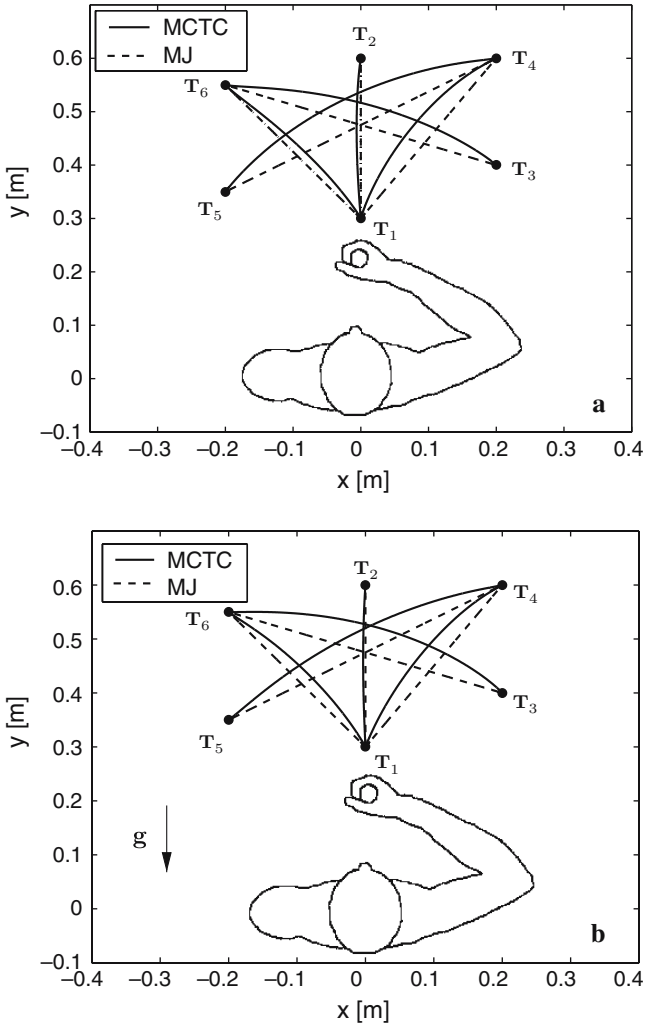

Fig. 8 Hand paths of movements in **a** *horizontal* plane and in **b** *vertical* plane resulting from the MCTC and the MJ models. In condition **b**, the subject is lying on his back performing movements against the direction of the gravitational field **g**. No significant difference in hand paths between conditions **a** and **b** can be observed

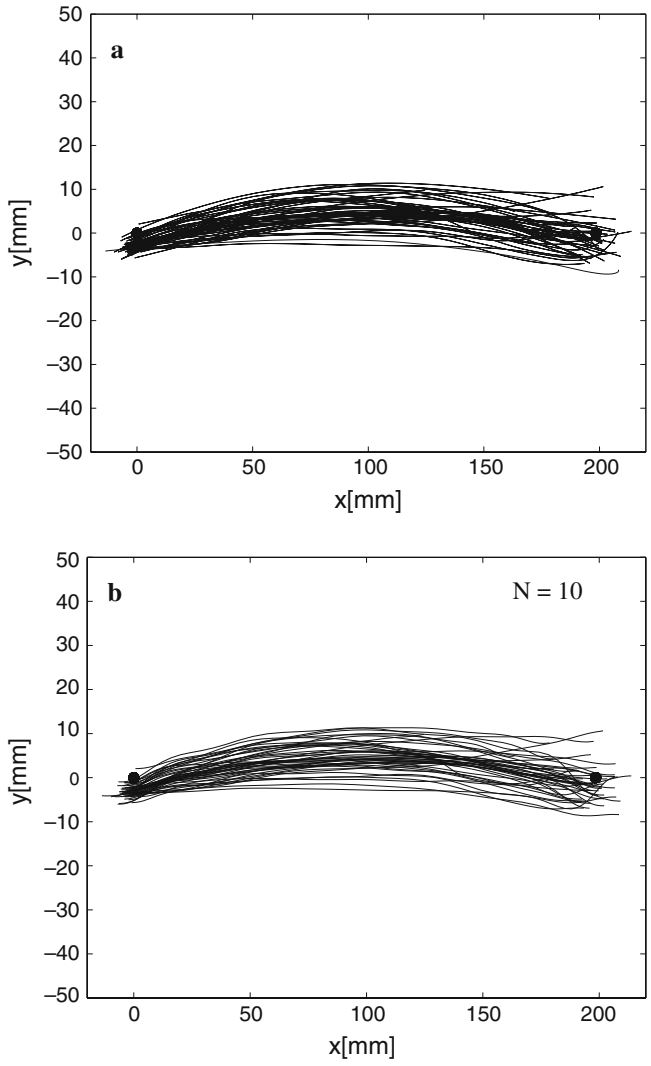

Fig. 9 **a** Experimentally measured hand paths between an initial target located at $\mathbf{x}_0 = (0, 0)^{\mathrm{T}}$ m and a final target located at $\mathbf{x}_{\mathrm{f}} = (0.2, 0)^{\mathrm{T}}$m. **b** Hand paths as they result from an expansion into a set of basis functions up to order $N = 10$ between the same targets as in **a**. The hand paths are recovered well in the low dimensional feature space

Table 4 Distance of hand paths in feature space between the MCTC model in the horizontal plane (MTCT(h)) and the minimum-jerk model (MJ) and the distance between hand paths derived from the MTCT model in the horizontal and vertical (MCTC(v)) conditions

Targets $\mathbf{x}_0 \rightarrow \mathbf{x}_{\mathrm{f}}$	Distance MJ – MCTC(h)	Distance MCTC(h) – MCTC(v)
$\mathbf{T}_1 \rightarrow \mathbf{T}_2$	0.0030	0.0000
$\mathbf{T}_1 \rightarrow \mathbf{T}_4$	0.0605	0.0090
$\mathbf{T}_1 \rightarrow \mathbf{T}_6$	0.0216	0.0100
$\mathbf{T}_3 \rightarrow \mathbf{T}_6$	0.0437	0.0115
$\mathbf{T}_5 \rightarrow \mathbf{T}_4$	0.0656	0.0197

Another application of the discrete representation consists of the low dimensional representation of movements. Figure 9a shows a set of experimentally measured hand paths in the horizontal plane between an initial and a final target. Figure 9b shows the hand paths between the same targets resulting from an expansion into a set of basis functions up to order $N = 10$. The original paths are recovered well in the low dimensional feature space.

2.6 Periodic tracing of planar shapes

This section presents two problems widely used in the study of human motor behavior involving periodic arm movements for which either no analytical solution or only asymptotics of solutions are known. First, a periodic tracing problem, in which the end-effector moves along an elliptical path, is considered.

2.6.1 Ellipse

The end-effector (hand) of a two-link planar arm tracks a given path in the shape of an ellipse (Fig. 10). Due to its

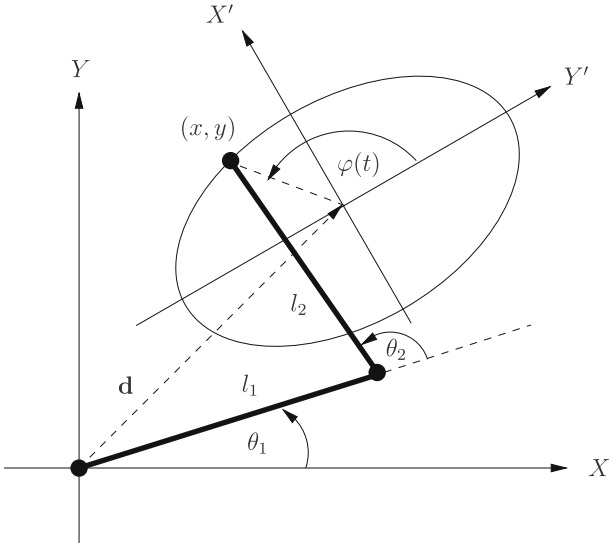

Fig. 10 Movement of an end-effector along an elliptical path

significance to human motor control the cost function is taken as the squared jerk of the end-effector integrated over the movement time (Flash and Hogan 1985). Periodic boundary conditions are imposed, corresponding to experimental settings, where the subject is instructed to trace the elliptical figures continuously without stopping.

The transformation of the end-effector from the ellipse-centered frame with coordinates $\mathbf{x}' = (x', y')$ to the shoulder frame with coordinates $\mathbf{x} = (x, y)$ is given by a rigid transformation

$$\mathbf{x} = R\mathbf{x}' + \mathbf{d} \tag{74}$$

with the rotation matrix R, $RR^{\mathrm{T}} = I$, and the translation vector $\mathbf{d}$.

The goal is to minimize

$$\mathcal{C} = \int_0^{\mathrm{T}} \left(\dddot{x}^2 + \dddot{y}^2 \right) \mathrm{d}t \tag{75}$$

subject to the constraint

$$\left(\frac{x'}{a}\right)^2 + \left(\frac{y'}{b}\right)^2 = 1. \tag{76}$$

The parameters a and b denote the semi-major and semi-minor axes of the ellipse, respectively, and the (squared) eccentricity of the ellipse is defined as $\varepsilon = (1 - b^2/a^2)$.

It is useful to express the functional (75) in the ellipse-centered coordinate system. It can easily be verified that the functional is invariant under the rigid transformation (74), leading to

$$\mathcal{C} = \int_0^{\mathrm{T}} \left(\dddot{x}^2 + \dddot{y}^2 \right) \mathrm{d}t = \int_0^{\mathrm{T}} \left(\dddot{x}'^2 + \dddot{y}'^2 \right) \mathrm{d}t. \tag{77}$$

By parameterizing the ellipse as

$$x' = a \cos\varphi, \tag{78}$$

$$y' = b \sin\varphi, \tag{79}$$

where φ is the rotation angle ($0 \le \varphi \le 2\pi$), the constraint (76) is identically satisfied.

Substituting (78) and (79) into the cost functional (77) gives

$$\mathcal{C} = \frac{a^2}{T^5} \int_0^1 \Big(\Big[-\varphi'^3 \sin\varphi + 3\varphi'\varphi'' \cos\varphi + \varphi^{(3)} \sin\varphi \Big]^2 + (1-\varepsilon) \Big[\varphi'^3 \cos\varphi + 3\varphi'\varphi'' \sin\varphi - \varphi^{(3)} \cos\varphi \Big]^2 \Big) \mathrm{d}\tau, \tag{80}$$

where the prime denotes the derivative with respect to normalized time $\tau = t/T$. The cost functional (80) is minimized subject to the boundary conditions $\varphi(0) = 0$, $\varphi(1) = 2\pi$ and periodic boundary conditions in the derivatives as specified in (4).

Applying a parameterization of the angle φ in the form (17) transforms the cost function into a scalar function of the expansion coefficients. The parameter optimization of the cost yields the results shown in Table 5 for different values of (squared) eccentricity ε with a semi-major axis of $a = 0.15\,\mathrm{m}$ and the period of the movement $T = 1\,\mathrm{s}$. The results of the multiple shooting algorithm with an initial guess provided by the solution of the parameter optimization method are shown on the right side of Table 5. It should be noted that the minimal value of the cost is identical for the two methods, indicating that the function and its derivatives appearing in the cost are recovered well with the parameterization method.

The analysis of handwriting and drawing movements of humans shows a close relation between the hand speed

$$v(t) = \sqrt{\dot{x}^2 + \dot{y}^2} \tag{81}$$

and the instantaneous curvature of the path

$$\kappa(t) = \frac{\dot{x}\ddot{y} - \dot{y}\ddot{x}}{\sqrt{\dot{x}^2 + \dot{y}^2}^3}. \tag{82}$$

In several experimental studies (Viviani and Terzuolo 1982; Laquaniti et al. 1983; Viviani and Flash 1995) it was found that this phenomena could be expressed in terms of a power law between absolute hand velocity and curvature (two-thirds power law),

$$v = g\kappa^{-\beta}, \tag{83}$$

where the accepted value of the exponent $\beta \simeq 0.33$ and g denotes the gain factor.

Table 5 Results of the optimization for movements along an elliptical path

Parameter optimization			Multiple shooting		
ε	N	$\mathcal{C}$	$E_{\max}$	$\mathcal{C}$	$E_{\max}$
0.1	20	1315.18	8.4e − 2	1315.18	3.1e − 14
0.2	20	1245.94	1.8e − 1	1245.94	6.1e − 14
0.5	20	1038.14	9.4e − 1	1038.14	1.6e − 13
0.7	20	899.50	4.5e + 1	899.50	2.5e − 13
0.9	20	760.70	7.3e + 2	760.70	1.1e − 12

Figure 11a shows the optimal speed profile for different values of (squared) eccentricity. The dependency of the speed on the instantaneous curvature was analyzed by the influence of the eccentricity on the exponent β. For a given eccentricity, the optimal angle trajectory was determined and a linear regression on the $\log(\kappa) - \log(v)$ data was performed, giving the exponent β as the slope of the fitted straight line.

For the case where the (squared) eccentricity of the ellipse is small, $\varepsilon \ll 1$, an analytical solution to the minimization of the cost, (77), under the constraint that a power law of the form (83) holds, was determined by Richardson and Flash (2002) using a perturbative approach. In this work, the exponent β is not specified a priori but is an outcome of the optimization. To a first-order approximation of the (squared) eccentricity, the solution is given according to Richardson and Flash (2002) by

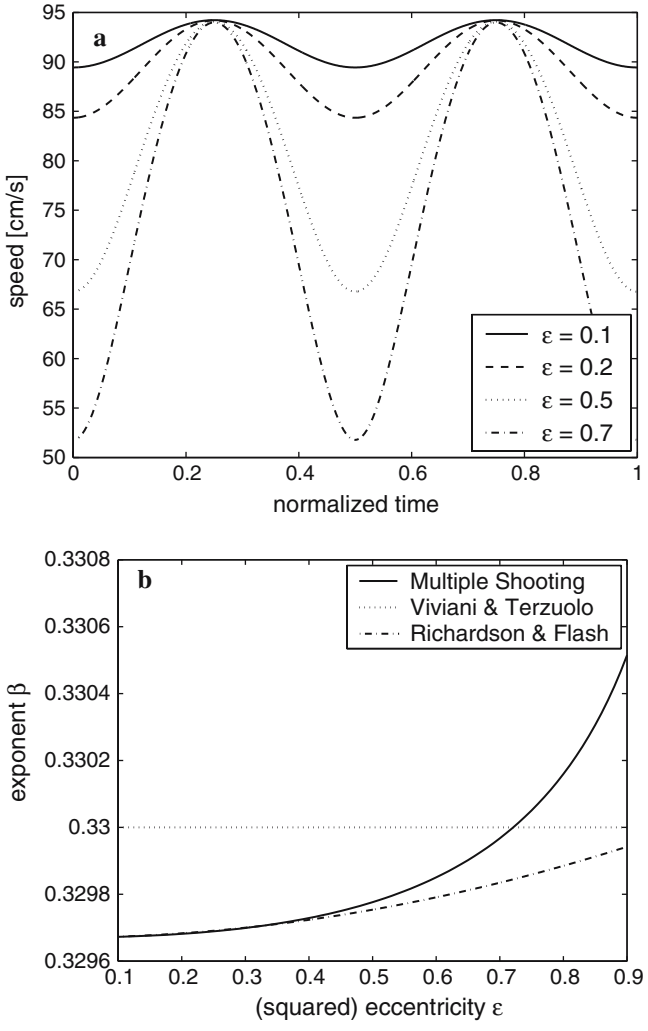

Fig. 11 **a** Optimal speed profiles for different values of (squared) eccentricity ε. **b** Exponent β as a function of (squared) eccentricity ε using a multiple shooting method for the optimization of the minimum-jerk cost along the elliptical path and the results obtained by Viviani and Terzuolo (1982) ($\beta \approx 0.33$) and Richardson and Flash (2002) ($\beta \approx 0.3297 + 0.000336\varepsilon^2$)

$$\varphi(\tau) = 2\pi\tau + \frac{\varepsilon}{8}(1 - 3\beta)\sin(4\pi\tau) \tag{84}$$

with a value of $\beta = 30/91 + 0.000336\varepsilon^2$ up to second-order ε^2. The analytically derived value for the exponent β is in excellent agreement with simulation results in the asymptotic limit of small values of ε, as shown in Fig. 11b.

The Fourier analysis of the optimal rotation angle shows that all coefficients vanish ($< 10\mathrm{e}-7$) except the coefficient a_2 which takes increasing values with increasing eccentricity (e.g., $a_2 = 0.0017$ for $\varepsilon = 0.1$, $a_2 = 0.0188$ for $\varepsilon = 0.7$). The periodic tracing of the ellipse can thus be represented as a one dimensional vector in Fourier space. This result is already expressed in the asymptotic limit $\varepsilon \ll 1$ given by (84).

In closing, the proposed approach verifies the known two-thirds power law result observed as humans trace elliptical paths. This result was obtained by applying the minimum-jerk model to an elliptical path for a wide range of elliptical shapes *without* additionally enforcing a power law of the form (83).

2.6.2 Cloverleaf

The tracing of a cloverleaf path, as shown in Fig. 12, defines another interesting problem in motor control research that has been measured experimentally (Viviani and Flash 1995). As in the case of an elliptical path we analyze the predictions of the minimum-jerk model when tracing periodically the shape of a cloverleaf. A cloverleaf can be represented as follows (Richardson and Flash 2000, 2002)

$$x' = \frac{a}{2}(\cos 3\varphi - \cos\varphi)\,, \tag{85}$$

$$y' = \frac{a}{2}(\sin 3\varphi + \sin\varphi)\,, \tag{86}$$

where φ is the rotation angle ($0 \le \varphi \le 2\pi$) and a defines the size of the leaf.

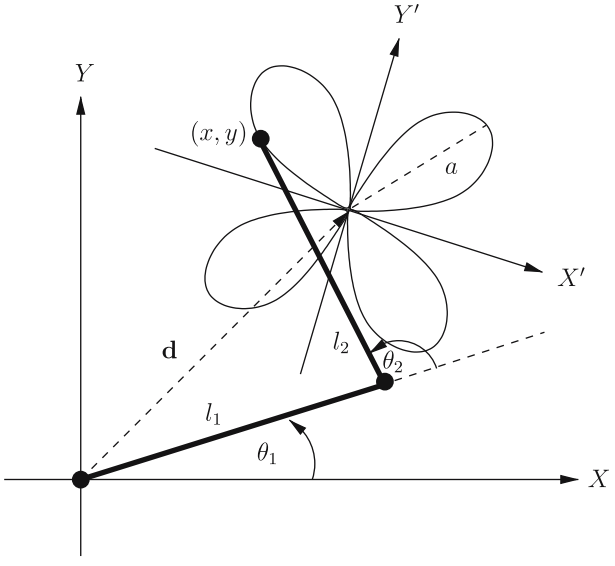

Fig. 12 Movement of an end-effector along a cloverleaf path

As in the case of an elliptical path the squared jerk cost is minimized along the cloverleaf path for a period of $T = 3\,\mathrm{s}$ and radius $a = 0.15\,\mathrm{m}$. The error of the optimal rotation angle is $E_{\max} = 1.6\mathrm{e}-13$ with minimal cost $\mathcal{C} = 1039.0$. The resulting optimal speed profile of the end-effector is shown in Fig. 13a.

To estimate the exponent of a possible power law, relating the speed v and the curvature κ, a linear regression on the $\log\kappa$ versus $\log v$ graph was applied. The value of the exponent derived from this curve was $\beta = 0.4252$ (Fig. 13b). This result does not agree well with the experimental findings by Viviani and Flash (1995). Cloverleafs that were traced with periods of 2.5 and 3 s were found to have average values of β of 0.35 ± 0.03 and 0.36 ± 0.03, respectively. Richardson and Flash (2002, 2000) determined a β coefficient of 0.4214 using the same perturbative approach as in the case of an elliptical path. However, this result was considered to be inaccurate since it was obtained in a limit where the perturbation approach fails. A numerical method was applied instead, leading to an exponent $\beta = 0.36 \pm 0.01$, which compares favorably with the experiments, but is in disagreement with the findings here.

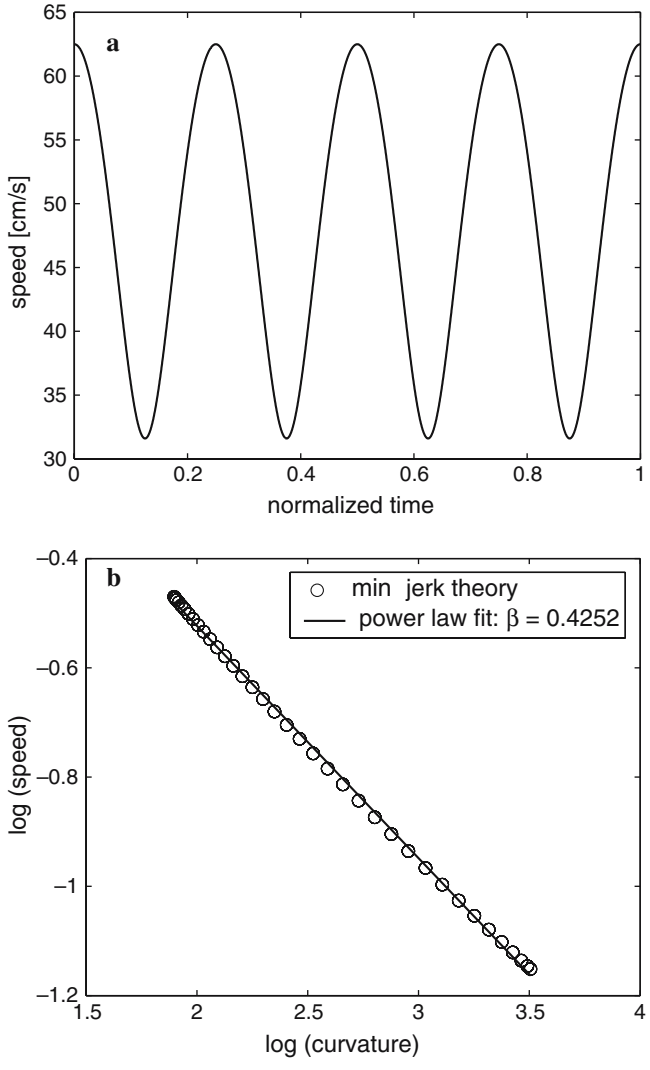

Fig. 13 **a** An optimal speed profile resulting from minimization of the squared jerk minimization along the cloverleaf path with movement period of $T = 3\,\mathrm{s}$. **b** The log(curvature) versus log(speed) curve as derived from the minimum-jerk theory and the power law fit. The value of the exponent obtained from this curve is $\beta = 0.4252$

The Fourier analysis of the optimal rotation angle shows that only two expansion coefficients differ significantly from zero, namely $a_4 = -0.0349$ and $a_8 = 0.0017$. The periodic tracing of the cloverleaf path using a minimum-jerk criterion can thus be represented as a two-dimensional vector in Fourier space.

2.7 Geodesics in configuration space of a four DOF arm

In this section, models related to point-to-point movements of a four DOF arm in three-dimensional space are presented. The joint angular paths of the movement are assumed to be geodesics in configuration space with respect to a metric defined by the manipulator inertia matrix. The geodesic paths correspond to arm movements without external forces. Such an approach is motivated by the experimental findings that inertial properties of the arm are important in the control of arm movements (Soechting et al. 1995; Flanders et al. 2003). Moreover, Shin and McKay (1986) proved that geodesics with respect to the manipulator matrix define minimum time paths, provided that the driving actuator torques follow a bang-bang control strategy.

It should be noted that geodesic paths only determine the geometrical properties of the movement (e.g., path, posture) and do not include the temporal aspects of the movement (e.g., speed). An additional model for the latter has to be defined in order to define the spatiotemporal properties of the movement. However, an approach based on the separation of temporal and geometrical properties of the movement is supported by experimental studies (Nishikawa et al. 1999; Flanders et al. 2003; Torres and Zipser 2002, 2004; Sosnik et al. 2004). Behavioral studies of point-to-point movements demonstrate that the hand path and arm postures chosen during movement do not significantly depend on hand speed suggesting that the geometrical and kinematic properties are decoupled. In addition, neurophysiological studies of reaching movements in monkeys showed that geometrical and temporal attributes in terms of the movement direction and the movement speed, respectively, are represented in the cortical activity (Georgopoulus et al. 1986; Moran and Schwartz 1999).

Geodesics in configuration space with respect to a metric defined by the manipulator inertia matrix are closely related to the kinetic energy which is computed first. For this purpose, an arm configuration is parameterized as in the work of Soechting et al. (1995) and defined by the four joint angles $\boldsymbol{\theta} := (\theta, \eta, \zeta, \phi)^{\mathrm{T}}$. The first three angles describe the rotation around the spherical shoulder joint, namely the elevation angle θ, the azimuthal angle η and the humeral angle ζ, whereas the flexion angle ϕ determines the rotation around

the revolute elbow joint (Fig. 14). It should be noted that the three DOF at the wrist can be neglected for pointing movements, but play a significant role in grasping studies. Two body-fixed coordinate systems are attached to the upper and forearm at the center of mass of each limb, such that the z axis is pointing along the longitudinal limb axis and the x and y axes are in transverse directions.

The kinetic energy of the arm with this choice of coordinates can then be expressed as (Biess et al. 2001)

$$\begin{aligned} T = \frac{1}{2}\Big[& I_1(\omega_{1,x}^2 + \omega_{1,y}^2) + I_2\omega_{1,z}^2 \\ & + I_3\left(\left(\omega_{1,y}\cos\phi + \omega_{1,z}\sin\phi\right)^2 + (\omega_{1,x} + \dot{\phi})^2\right) \\ & + I_4\left(\omega_{1,z}\cos\phi - \omega_{1,y}\sin\phi\right)^2 \\ & + 2A(\omega_{1,y}^2\cos\phi + \omega_{1,x}^2\cos\phi + \omega_{1,y}\omega_{1,z}\sin\phi \\ & + \omega_{1,x}\dot{\phi}\cos\phi)\Big], \end{aligned} \tag{87}$$

where the angular velocity components of the upper arm with respect to the upper arm body coordinate system are

$$\omega_{1,x} = \dot{\eta}\sin\zeta\sin\theta + \dot{\theta}\cos\zeta, \tag{88}$$

$$\omega_{1,y} = \dot{\eta}\cos\zeta\sin\theta - \dot{\theta}\sin\zeta, \tag{89}$$

$$\omega_{1,z} = \dot{\eta}\cos\theta + \dot{\zeta}. \tag{90}$$

The constants are defined by

$$I_1 = I_{1,x} + m_1 r_1^2 + m_2 l_1^2, \tag{91}$$

$$I_2 = I_{1,z}, \tag{92}$$

$$I_3 = I_{2,x} + m_2 r_2^2, \tag{93}$$

$$I_4 = I_{2,z}, \tag{94}$$

$$A = m_2 l_1 r_2, \tag{95}$$

where $m_i, I_{i,x}, I_{i,y}, I_{i,z}, l_i, r_i, (i = 1, 2)$, denote mass, principal moments of inertia around the x, y, z axes of the body-fixed coordinate systems, length and distance to the center of mass of the upper and forearm, respectively. It is assumed that the principal moments of inertia around axes transverse to the limbs are identical, i.e., $I_{1,x} = I_{1,y}$ and $I_{2,x} = I_{2,y}$.

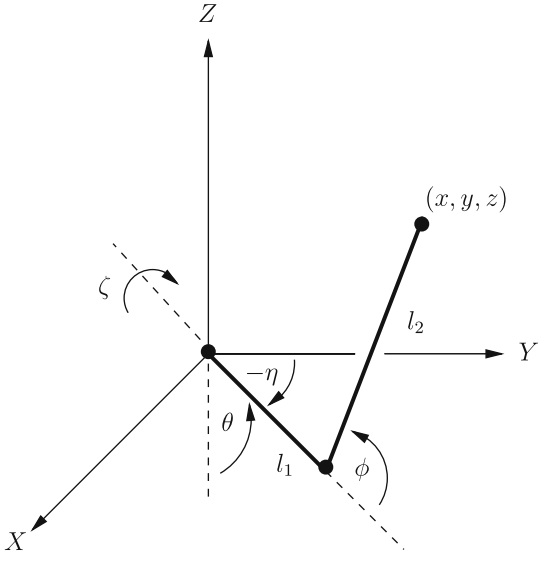

Fig. 14 A mechanical linkage model of a four DOF arm

The kinetic energy is a quadratic form in the joint velocities and can be written as

$$T(\boldsymbol{\theta}, \dot{\boldsymbol{\theta}}) = \frac{1}{2}\dot{\boldsymbol{\theta}}^{\mathrm{T}} M(\boldsymbol{\theta})\dot{\boldsymbol{\theta}}, \tag{96}$$

where $M \in \mathbb{R}^{4\times4}$ is the manipulator inertia matrix with components given in Appendix B. The manipulator inertia matrix depends on the current configuration and represents the instantaneous composite mass distribution of the whole arm linkage at the current arm configuration (Asada and Slotine 1986).

Geodesics with respect to a metric defined by the manipulator matrix can be derived as extremals of the functional given by

$$\mathcal{C} = \frac{1}{2}\int_0^1 \boldsymbol{\theta}'^{\mathrm{T}}(\lambda) M(\boldsymbol{\theta}(\lambda))\boldsymbol{\theta}'(\lambda)\mathrm{d}\lambda \tag{97}$$

with boundary conditions

$$\boldsymbol{\theta}(0) = \boldsymbol{\theta}_0, \qquad \boldsymbol{\theta}(1) = \boldsymbol{\theta}_{\mathrm{f}}, \tag{98}$$

where $\boldsymbol{\theta}_0$ and $\boldsymbol{\theta}_{\mathrm{f}}$ denote the initial and final joint configuration, respectively, and the prime denotes derivative with respect to the path parameter, λ, in configuration space. The path in configuration space, $\boldsymbol{\theta} = \boldsymbol{\theta}(\lambda)$, satisfies the Euler–Lagrange equations which have the form of geodesic equations,

$$M(\boldsymbol{\theta})\boldsymbol{\theta}'' + C(\boldsymbol{\theta}, \boldsymbol{\theta}')\boldsymbol{\theta}' = 0, \tag{99}$$

where the components of the Coriolis matrix are given by

$$C_{ij}(\boldsymbol{\theta}, \boldsymbol{\theta}') = \frac{1}{2}\sum_{k=1}^{4}\left(\frac{\partial M_{ij}}{\partial\theta_k} + \frac{\partial M_{ik}}{\partial\theta_j} - \frac{\partial M_{kj}}{\partial\theta_i}\right)\theta_k'. \tag{100}$$

The influence of a gravity field $\mathbf{g}$ can be modeled by considering the potential energy of the arm. The potential energy of the arm is given by the sum of the potential energies of the upper arm and forearm

$$V = V_1 + V_2 = m_1 g h_1 + m_2 g h_2, \tag{101}$$

where h_1 and h_2 are the heights of the center of mass of the upper and forearm, respectively. Expressing the heights in terms of the joint angles and the limb lengths, the potential energy is

$$\begin{aligned} V(\boldsymbol{\theta}) = {} & g m_1 r_1 - g m_1 r_1\cos\theta + g m_2(l_1 + r_2) \\ & - g m_2\left[l_1\cos\theta + r_2(\cos\phi\cos\theta \right. \\ & \left. - \cos\zeta\sin\phi\sin\theta)\right], \end{aligned} \tag{102}$$

where a constant term was added such that the zero level of the potential energy corresponds to the zero configuration

($\theta = \eta = \zeta = \phi = 0$) of the arm. To model the influence of gravity the functional (97) is increased by the potential term

$$\mathcal{C}_w = \int_0^1 \left[\frac{1}{2} \boldsymbol{\theta}'^{\mathrm{T}}(\lambda) M(\boldsymbol{\theta}(\lambda)) \boldsymbol{\theta}'(\lambda) \mathrm{d}\lambda + w V(\boldsymbol{\theta}(\lambda)) \right] \mathrm{d}\lambda \tag{103}$$

The parameter w is a weighting factor between 0 and 1 that accounts for the influence of the gravitational field.

The physical parameters of the arm that are used in the simulation studies are given in Table 6. An expansion of the form $m = 1$ is assumed for the joint angular paths. The optimization results are shown in Table 7. The joint angular paths between two configurations as a function of the path parameter λ are shown in Fig. 15.

The end-effector path can be determined from the joint trajectories via the forward kinematics

$$\begin{aligned} x &= -l_1 \sin\eta \sin\theta - l_2[\cos\phi \sin\eta \sin\theta \\ &\quad + \sin\phi\,(\cos\zeta \sin\eta \cos\theta + \sin\zeta \cos\eta)], \end{aligned} \tag{104}$$

$$\begin{aligned} y &= l_1 \cos\eta \sin\theta + l_2[\cos\phi \cos\eta \sin\theta \\ &\quad + \sin\phi\,(\cos\zeta \cos\eta \cos\theta - \sin\zeta \sin\eta)], \end{aligned} \tag{105}$$

$$z = -l_1 \cos\theta + l_2\,[\sin\phi \cos\zeta \sin\theta - \cos\phi \cos\theta]\,. \tag{106}$$

The comparison of the predictions of the geodesics model with the experimental data can be found in Biess (2004)

Table 6 Parameters for the arm model used in the simulation of geodesics

Parameter	Shoulder joint ($i = 1$)	Elbow joint ($i = 2$)
Mass: m_i (kg)	2.185	1.64
Length: l_i (m)	0.30	0.32
Distance to center of mass: r_i (m)	0.15	0.16
Moment of inertia around x axis: $I_{i,x}$ (kg m^2)	0.0983	0.0840
Moment of inertia around z axis: $I_{i,z}$ (kg m^2)	0.0164	0.0140

Table 7 Results of the optimization for the cost $\mathcal{C}$ and $\mathcal{C}_{w=1}$ in configuration space between different arm configurations (in rad)

Config	Parameter Optimization			Multiple Shooting	
$\boldsymbol{\theta}_0 \to \boldsymbol{\theta}_\mathrm{f}$	N	$\mathcal{C}$	Emax	$\mathcal{C}$	Emax
$\boldsymbol{\theta}_1 \to \boldsymbol{\theta}_2$	10	0.1265	9.4e − 3	0.1265	1.1e − 16
$\boldsymbol{\theta}_1 \to \boldsymbol{\theta}_3$	10	0.4537	4.0e − 2	0.4537	3.3e − 16
$\boldsymbol{\theta}_1 \to \boldsymbol{\theta}_4$	10	0.4235	5.1e − 2	0.4235	3.6e − 16
$\boldsymbol{\theta}_2 \to \boldsymbol{\theta}_3$	10	0.4592	9.2e − 2	0.4592	2.2e − 16
$\boldsymbol{\theta}_2 \to \boldsymbol{\theta}_4$	10	0.1085	2.0e − 2	0.1085	8.3e − 17
$\boldsymbol{\theta}_3 \to \boldsymbol{\theta}_4$	10	0.7770	9.9e − 2	0.7770	2.1e − 16
$\boldsymbol{\theta}_0 \to \boldsymbol{\theta}_\mathrm{f}$	N	$\mathcal{C}_{w=1}$	Emax	$\mathcal{C}_{w=1}$	Emax
$\boldsymbol{\theta}_1 \to \boldsymbol{\theta}_2$	15	4.827	2.1e − 1	4.827	4.6e − 15
$\boldsymbol{\theta}_1 \to \boldsymbol{\theta}_3$	15	9.228	2.6e − 1	9.228	6.2e − 15
$\boldsymbol{\theta}_1 \to \boldsymbol{\theta}_4$	15	3.897	6.3e − 1	3.897	4.4e − 15
$\boldsymbol{\theta}_2 \to \boldsymbol{\theta}_3$	15	8.059	2.3e + 0	8.059	6.2e − 17
$\boldsymbol{\theta}_2 \to \boldsymbol{\theta}_4$	15	2.793	2.0e − 1	2.793	4.6e − 15
$\boldsymbol{\theta}_3 \to \boldsymbol{\theta}_4$	15	7.109	1.1e + 0	7.109	6.8e − 15

$\boldsymbol{\theta}_1 = (\pi/2, -\pi/4, \pi/4, \pi/12)^\mathrm{T}$, $\boldsymbol{\theta}_2 = (\pi/3, -\pi/12, \pi/8, \pi/4)^\mathrm{T}$, $\boldsymbol{\theta}_3 = (3\pi/4, \pi/12, \pi/12, \pi/6)^\mathrm{T}$, $\boldsymbol{\theta}_4 = (\pi/4, \pi/12, \pi/6, \pi/12)^\mathrm{T}$

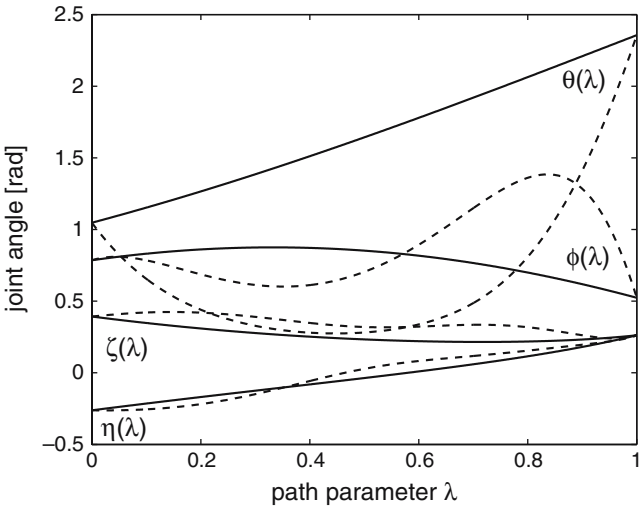

Fig. 15 Optimal joint trajectories $\boldsymbol{\theta} = (\theta, \eta, \zeta, \phi)^\mathrm{T}$ as a function of the path parameter λ resulting from the minimization of the cost $\mathcal{C}$ (*solid line*) and $\mathcal{C}_{w=1}$ (*dashed line*), respectively, with initial arm configuration $\boldsymbol{\theta}_0 = (\pi/3, -\pi/12, \pi/8, \pi/4)^\mathrm{T}$rad and final arm configuration $\boldsymbol{\theta}_\mathrm{f} = (3\pi/4, \pi/12, \pi/12, \pi/6)^\mathrm{T}$rad

and will be reported in detail in a subsequent paper. In this work, we focused on the computational methods involved in the derivation of the optimal solution. Nevertheless, several examples of the wrist path for four different subjects and a comparsion with the predictions of the geodesics model are presented in Fig. 16a.

Finally, Fig. 17 shows several examples for which the gravitational potential with a weighting coefficient $w = 1$ is included into the cost function. The predicted paths are strongly curved in the direction of the gravitational field and therefore do not provide a good description of the experimental data.

2.7.1 Redundancy resolution at the final target

The previously computed geodesics were completely specified in configuration space. However, a pointing task is generally expressed in work-space by three Cartesian coordinates of the final target location $\mathbf{x}_\mathrm{f}$. In the following section, we derive the hand path and the final arm configuration simultaneously from geodesics by specifying only the final hand location, i.e., by replacing the boundary condition (98) with

$$\boldsymbol{\theta}(0) = \boldsymbol{\theta}_0, \qquad \mathbf{x}_\mathrm{h}(1) = \mathbf{x}_\mathrm{f}, \tag{107}$$

where $\mathbf{x}_\mathrm{h}$ denotes the hand location. Due to the excess of one DOF in configuration space a given hand location does not determine an arm configuration completely (redundancy). Indeed, for a fixed hand location the arm can still rotate around an axis going to the shoulder and the hand location, implying that the elbow location is constrained to a circle around this axis. The redundancy at the final target can be resolved using geodesics. For this purpose, the set of arm configurations that is compatible with the given hand location is determined (inverse kinematic map). The inverse kinematic map

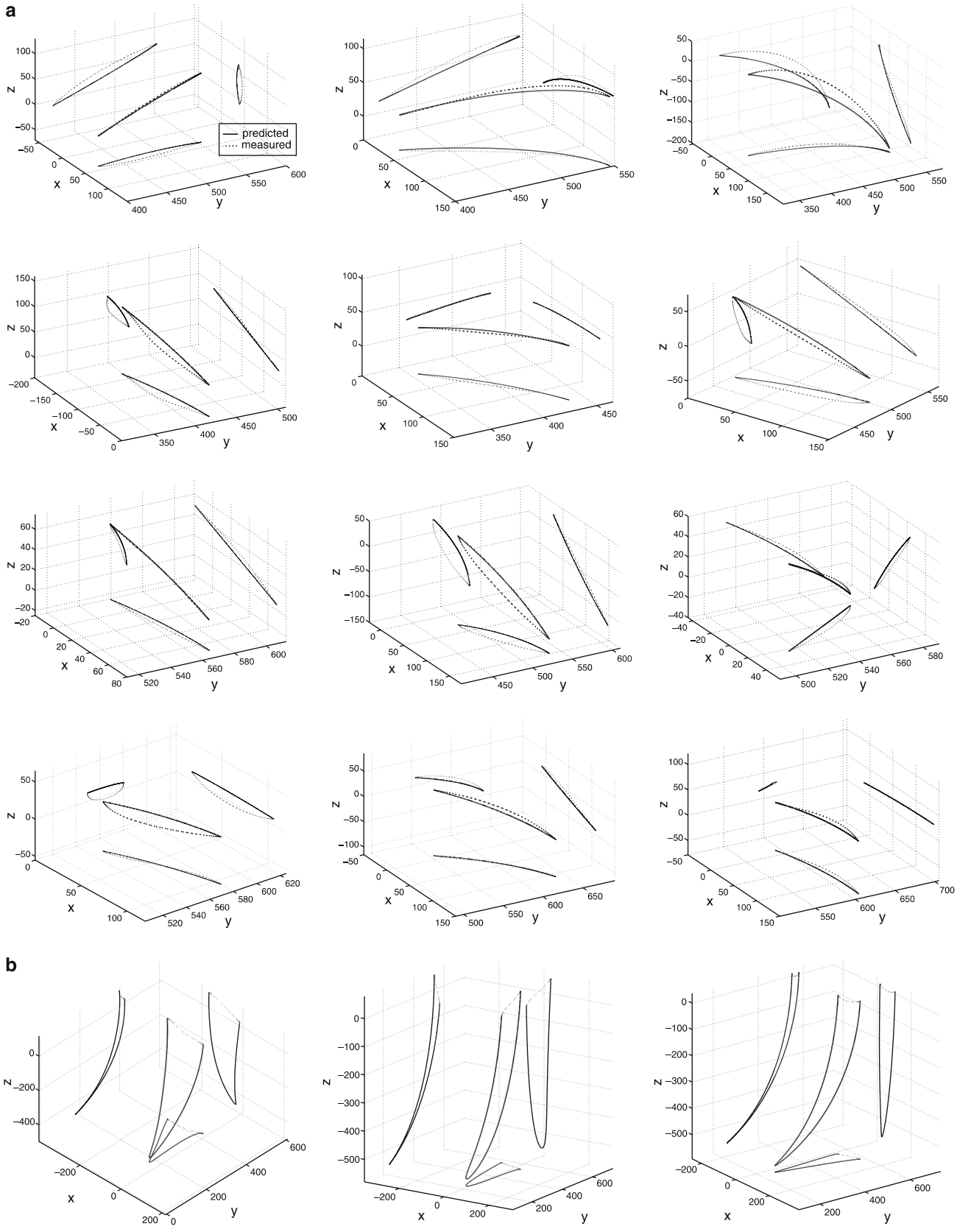

Fig. 16 **a** Examples of predicted three-dimensional wrist paths (*solid*) as derived from geodesics in configuration space and the measured wrist paths (dotted) in units of mm. The projections of the predicted (*solid*) and measured (*dotted*) paths in the xy, xz and yz plane are shown for visualization purposes. Each *row* represents a different subject. **b** Examples of predicted three-dimensional wrist paths (*solid*) as derived from the cost function including the gravitational potential, $\mathcal{C}_{w=1}$, and the measured wrist paths (*dotted*) in units of mm

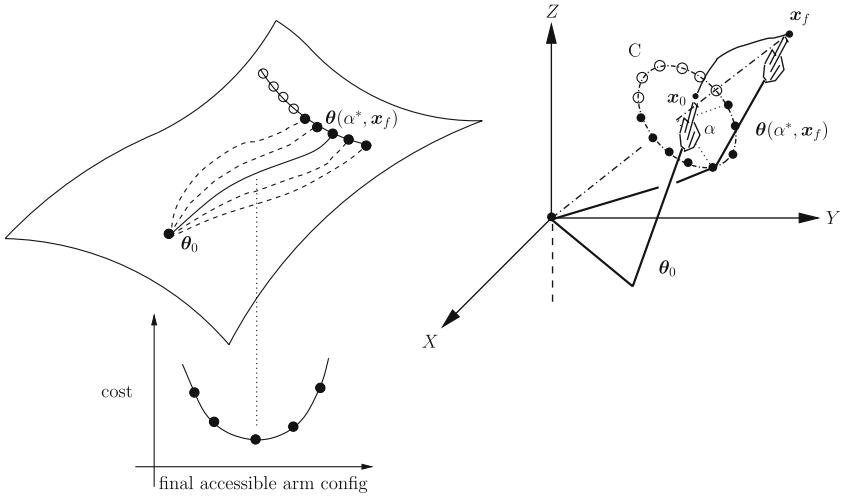

Fig. 17 Computation of the one-dimensional family of geodesics between the initial configuration $\boldsymbol{\theta}_0$ and the final configurations $\boldsymbol{\theta}_\mathrm{f}(\alpha, \mathbf{x}_\mathrm{f})$, $\alpha \in I(\mathbf{x}_\mathrm{f})$, that are compatible with the given final target location $\mathbf{x}_\mathrm{f}$. The configuration space (*left*) is represented as a two-dimensional surface. Each point in configuration space corresponds to an arm configuration. The cirle *C* in workspace (*right*) contains the final elbow locations inside (closed circle) and outside (open circle) of the bio-mechanical admissible joint range. The optimal geodesic (for $\alpha = \alpha^*$) in configuration space has the minimal cost over all accessible final arm configurations and leads in workspace to an optimal hand path and an optimal final arm posture

has the form $\boldsymbol{\theta} = \boldsymbol{\theta}(\alpha, \mathbf{x}_\mathrm{h})$, where $\alpha \in [0, 2\pi)$ denotes the rotation angle of elbow locations on the circle, and is computed in two steps. First, the elbow locations are expressed as $\mathbf{x}_\mathrm{e} = \mathbf{x}_\mathrm{e}(\alpha, \mathbf{x}_\mathrm{h})$ by noting that the circle of elbow locations for a given hand location is determined by the intersection of the sphere $S_1 : \mathbf{x}^2 = l_1^2$ around the origin with radius l_1 and the sphere $S_2 : (\mathbf{x} - \mathbf{x}_\mathrm{h})^2 = l_2^2$ around the hand location $\mathbf{x}_\mathrm{h}$ with radius l_2. Second, an arm configuration is uniquely determined by a given elbow *and* hand location, i.e., there exists a relation of the form $\boldsymbol{\theta} = \boldsymbol{\theta}(\mathbf{x}_\mathrm{e}, \mathbf{x}_\mathrm{h})$ or explicitly for our choice of coordinates ($|\mathbf{x}_\mathrm{e} \times \mathbf{x}_\mathrm{h}| \neq 0$ and $|z_\mathrm{e}| < l_u$):

$$\theta = \arccos\left(\frac{-z_\mathrm{e}}{l_u}\right) \tag{108}$$

$$\eta = \arctan2\,(-x_\mathrm{e}, y_\mathrm{e}) \tag{109}$$

$$\zeta = \arctan2\Big(l_u(x_\mathrm{e}y_\mathrm{h} - x_\mathrm{h}y_\mathrm{e}), \; y_\mathrm{e}(y_\mathrm{e}z_\mathrm{h} - y_\mathrm{h}z_\mathrm{e}) - x_\mathrm{e}(z_\mathrm{e}x_\mathrm{h} - z_\mathrm{h}x_\mathrm{e})\Big) \tag{110}$$

$$\phi = \arccos\left(\frac{x_\mathrm{h}^2 + y_\mathrm{h}^2 + z_\mathrm{h}^2 - l_u^2 - l_\mathrm{f}^2}{2l_u l_\mathrm{f}}\right), \tag{111}$$

where $\mathbf{x}_\mathrm{e} = (x_\mathrm{e}, y_\mathrm{e}, z_\mathrm{e})^\mathrm{T}$ and $\mathbf{x}_\mathrm{h} = (x_\mathrm{h}, y_\mathrm{h}, z_\mathrm{h})^\mathrm{T}$.

The inverse kinematic map follows then as $\boldsymbol{\theta}(\mathbf{x}_\mathrm{e}, \mathbf{x}_\mathrm{h}) = \boldsymbol{\theta}(\mathbf{x}_\mathrm{e}(\alpha, \mathbf{x}_\mathrm{h}), \mathbf{x}_\mathrm{h}) =: \boldsymbol{\theta}(\alpha, \mathbf{x}_\mathrm{h})$, defining a one-parameter family of arm configurations for a given hand location. Obviously not every rotation angle $\alpha \in [0, 2\pi)$ leads to a realistic arm posture. We determine next the subset of rotation angles that leads to postures inside the biomechanically admissible joint-range of the arm. We assume that only joint angles which satisfy the following inequalities lead to admissible arm configurations

$$0 \leq \theta(\alpha) \leq \pi, \tag{112}$$

$$-\frac{3}{4}\pi \leq \eta(\alpha) \leq \frac{\pi}{3}, \tag{113}$$

$$\zeta_\mathrm{ext}(\theta, \eta) \leq \zeta(\alpha) \leq \zeta_\mathrm{int}(\theta, \eta), \tag{114}$$

$$0 < \phi < \pi, \tag{115}$$

where the external and internal humeral rotation of the upper arm, ζ_ext and ζ_int, are experimentally determined functions (Wang et al. 1998). The external and internal humeral rotations describe the minimal and maximal measured value of the humeral angle for a given upper arm direction. These constraints define for each hand location in space, $\mathbf{x}_\mathrm{h}$, the interval of possible rotations angles, $I(\mathbf{x}_\mathrm{h}) \supset \alpha$. The corresponding joint angular vector associated with realistic arm postures at the final hand location $\mathbf{x}_\mathrm{f}$ is thus specified by the one-parameter family of vectors $\boldsymbol{\theta}(\alpha) = \boldsymbol{\theta}(\alpha, \mathbf{x}_\mathrm{f})$, $\alpha \in I(\mathbf{x}_\mathrm{f})$.

For the resolution of the redundancy at the final target location, the geodesics between the given initial arm configuration and the set of final arm configurations compatible with the given target location are computed. As a result, a one-parameter family of geodesics is obtained and the optimal path in configuration space is chosen as the geodesic with minimal length over all accessible final arm configurations. The optimal geodesic leads in workspace to an optimal hand path and an optimal final arm posture (Fig. 17). Figure 18 shows the results of the comparison between the predicted and the measured final arm configurations. The model prediction of the final arm postures provides a good fit for the experimental data as indicated by the r^2 values.

3 Discussion

The description of human arm behavior in terms of concise mathematical models is an important step toward a more

complete understanding of the human motor control system. Optimization principles based on deterministic performance indices have been proven to be useful tools in formulating coarse models of the motor behavior. The computation of the optimal solution is an essential part of any optimization model, and can be challenging depending on the complexity and order of the model. The representation of movements in the motor system is another open question. It is assumed that the observed motor patterns can be decomposed into simpler units. However, it is still unclear whether such motor primitives exist and how they can be defined.

In this work, these problems were addressed as follows. First, a robust, numerical method for the minimization of nonlinear performance indices was presented and applied to several problems in motor control theory. Second, a low dimensional representation of discrete (point-to-point) and rhythmic movements in terms of expansion coefficients of suitable sets of basis functions was introduced. The presented method can be used to explore the trajectories corresponding to different performance indices in order to test alternative hypotheses about movements. Results of simulation studies demonstrate the utility of the approach for studying the kinematics and dynamics of human arm movements.

The optimal solutions of the minimization of nonlinear cost functions were computed by a hybrid method consisting of a parameter optimization method combined with a multiple shooting algorithm. A series expansion of the generalized coordinates in terms of Jacobi polynomials was selected for the description of discrete (point-to-point) movements due to their compatibility with the imposed boundary conditions. Other complete sets of orthogonal polynomials, such as Chebyshev, Laguerre or Hermite polynomials, do not satisfy the boundary conditions. For rhythmic movements with periodic boundary conditions, a Fourier series expansion was used.

The two distinct expansion schemes – one for rhythmic and one for discrete movements – are mathematically a result of the different boundary conditions imposed. It is interesting to observe that the different settings at the boundaries correspond to biological differences in brain activity as shown in fMRI studies (Schaal et al. 2004). The movement initiation and termination in discrete movements is associated with an increase in cerebral brain activity compared to rhythmic movements. It was claimed that this difference may indicate that discrete movements invoke higher planning areas and thus require cognitive control whereas rhythmic movements are characterized by automatic control involving mainly primary motor circuits (Schaal et al. 2004).

It is important to note that an algorithm based exclusively on a parameter optimization method did not lead to trajectories that satisfied the necessary condition with high accuracy. This was related to the fact that higher derivatives of the series converged slowly (if at all) to the exact solution. If the objective is to determine the optimal solution for the position and velocity only, the results of the parameter optimization method may provide a sufficient approximation.

All presented examples resulted in solutions that satisfy the necessary condition of optimality to high accuracy. The analysis of the minimum commanded torque change model has led to results similar to those obtained by Wada et al. (2001), but did not require the tedious linearization of the Euler–Lagrange equations. Similar results for the hand paths were obtained for movements with and without the influence of gravity, suggesting that the minimum commanded torque change model is insensitive to the gravitational field.

The numerical analysis of movements involving the continuous tracing of an elliptical path while obeying a minimum-jerk criteria reproduced the analytical results obtained by Richardson and Flash (2002) in the asymptotic limit of small eccentricity. Moreover, it could be shown that the asymptotic results can be extended in good approximation to large eccentricities. A two-third power law could not be recovered for the tracing of a cloverleaf path using a minimum-jerk criteria which is in contrast to the findings of Richardson and Flash (2002). A Fourier analysis of the optimal solution showed that the periodic tracing of an elliptical path can be represented by only one expansion coefficient, whereas the tracing of a cloverleaf path required two coefficients. These movements can thus be generated by activating different frequency modes. It remains an open question whether the motor system makes use of such a representation and whether these expansion coefficients can be related to a set of motor primitives.

An important application of the feature space to the analysis of human movements consisted of the definition of a distance measure that allowed the quantitative comparison between the predictions (optimal solutions) of different models or the comparison between predictions and experimental data. For example, it is still debated whether the minimum-jerk model or the minimum commanded torque change model provides a better description for planar point-to-point movements. A comparison based on the suggested quantitative distant measure might finally resolve this ambiguity.

The presented algorithm has several limitations. The fact that the optimal solution satisfies the necessary conditions of optimality with high accuracy does not guarantee that the solution minimizes the performance index. It can be shown that the optimal solution is a minimum if the second variation of the cost functional is strictly positive (Gelfand and Fomin 1963). However, the numerical analysis of the second variation is not a trivial task (Galicki 1995) and was thus not considered in this work. Equality constraints were only incorporated in the case where they could be removed by rewriting the cost function in terms of a new set of coordinates without constraints. Inequality constraints appear naturally in modeling limb systems due to the limitations of the biomechanical joint range, but were not considered here.

The trajectory planning and control of artificial systems, such as humanoid robots, may benefit from the analysis of the movements in the low dimensional feature space of expansion coefficients. The successful recognition and classification of movements depend significantly on the selected feature space.

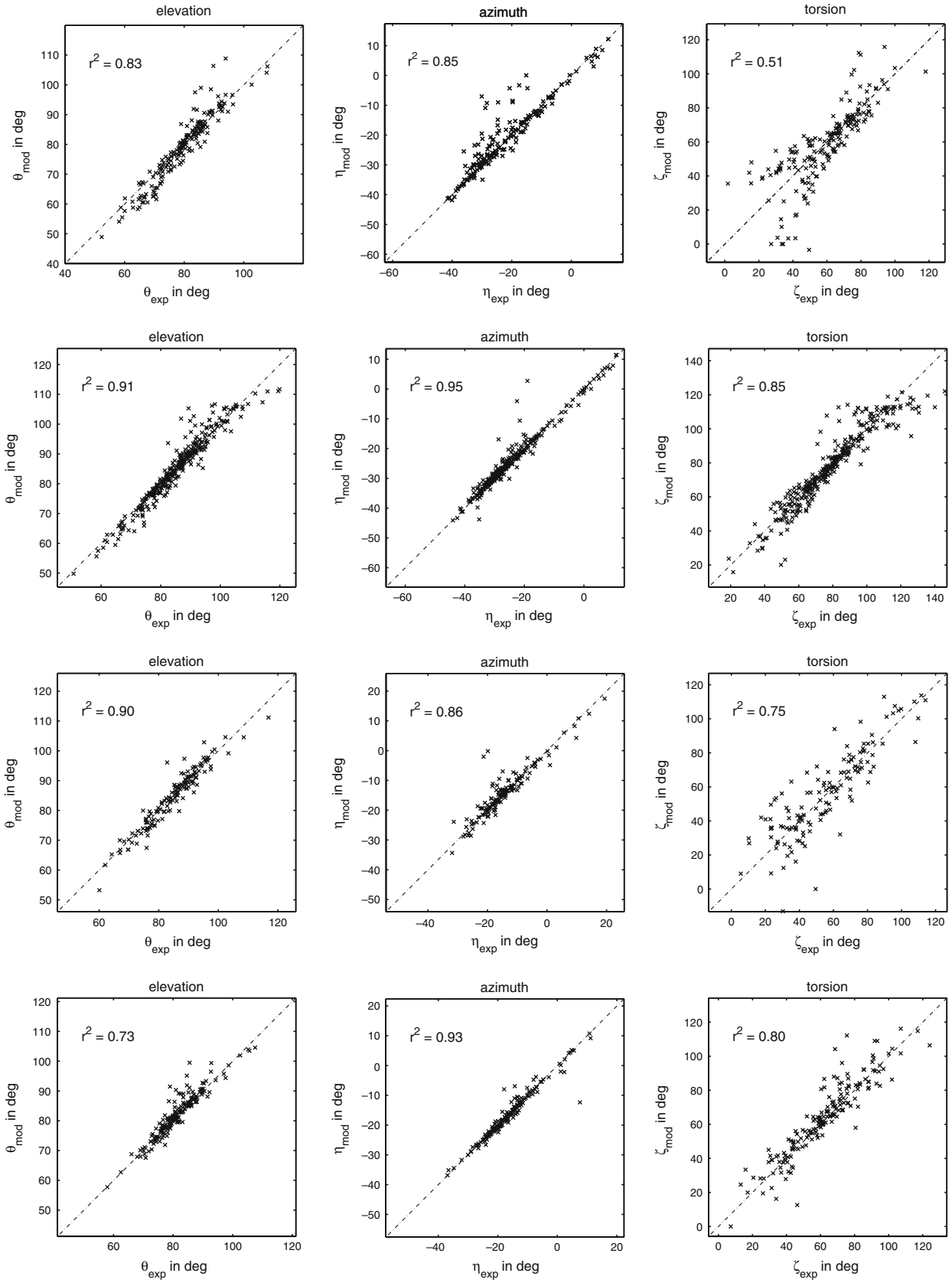

Fig. 18 Comparison of the model predictions for the elevation, azimuth and torsion angle ($\theta_{\mathrm{mod}}, \eta_{\mathrm{mod}}, \zeta_{\mathrm{mod}}$) with the experimental data ($\theta_{\mathrm{exp}}, \eta_{\mathrm{exp}}, \zeta_{\mathrm{exp}}$). Each row represents a different subject. A good fit is obtained as indicated by the r^2-values

In future work, the proposed approach will be applied to the study of human behavior by comparing real human movement data with the outcome of a theoretical model, defined by different performance indices.

Acknowledgements This research was supported in part by the German-Israeli Project Cooperation (DIP) and by the Moross Laboratory at the Weizmann Institute of Science. A. Biess is grateful to the Minerva Foundation which supported this research. M. Nagurka is grateful for a Fulbright scholarship allowing him to pursue this research. T. Flash is an incumbent of the Dr. Hymie Morros Professional chair.

Appendix A

Polynomial expansion

The coefficients of the polynomial appearing in the expansion schemes (5) for $m = 1, 2, 3$ are given by $2n$, $4n$ and $6n$ parameters, respectively, as follows:

$m = 1$:

$$\left.\begin{aligned} p_{i0} &= q_{i0} \\ p_{i1} &= q_{i\mathrm{f}} - q_{i0} \end{aligned}\right\}, \tag{116}$$

$m = 2$:

$$\left.\begin{aligned} p_{i0} &= q_{i0} \\ p_{i1} &= \dot{q}_{i0}T \\ p_{i2} &= 3(q_{i\mathrm{f}} - q_{i0}) - T(2\dot{q}_{i0} + \dot{q}_{i\mathrm{f}}) \\ p_{i3} &= -2(q_{i\mathrm{f}} - q_{i0}) + T(\dot{q}_{i0} + \dot{q}_{i\mathrm{f}}) \end{aligned}\right\}, \tag{117}$$

$m = 3$:

$$\left.\begin{aligned} p_{i0} &= q_{i0} \\ p_{i1} &= \dot{q}_{i0}T \\ p_{i2} &= \tfrac{1}{2}\ddot{q}_{i0}T^2 \\ p_{i3} &= \tfrac{1}{2}\big[20(q_{i\mathrm{f}} - q_{i0}) - 4(2\dot{q}_{i\mathrm{f}} + 3\dot{q}_{i0})T \\ &\quad +(\ddot{q}_{i\mathrm{f}} - 3\ddot{q}_{i0})T^2\big] \\ p_{i4} &= \tfrac{1}{2}\big[-30(q_{i\mathrm{f}} - q_{i0}) + 2(7\dot{q}_{i\mathrm{f}} + 8\dot{q}_{i0})T \\ &\quad -(2\ddot{q}_{i\mathrm{f}} - 3\ddot{q}_{i0})T^2\big] \\ p_{i5} &= \tfrac{1}{2}\big[12(q_{i\mathrm{f}} - q_{i0}) - 6(\dot{q}_{i\mathrm{f}} + \dot{q}_{i0})T \\ &\quad +(\ddot{q}_{i\mathrm{f}} - \ddot{q}_{i0})T^2\big] \end{aligned}\right\}, \tag{118}$$

where $i = 1, \ldots, n$ and $q_{i0}, q_{i\mathrm{f}}, \dot{q}_{i0}, \dot{q}_{i\mathrm{f}}, \ddot{q}_{i0}, \ddot{q}_{i\mathrm{f}}$ denote the generalized coordinates, velocities and accelerations at the beginning and the end of the movement, respectively, and T is the total movement time.

Appendix B

Manipulator inertia matrix

The components of the manipulator inertia matrix $M = (M_{ij})$ in the coordinates $\boldsymbol{\theta} = (\theta, \eta, \zeta, \phi)^{\mathrm{T}}$ are given by

$$\begin{aligned} M_{11} &= I_1 + 2A\cos\phi + I_3\cos^2\zeta + I_3\cos^2\phi\sin^2\zeta \\ &\quad +I_4\sin^2\phi\sin^2\zeta \\ M_{12} &= -\big[(A + (I_3 - I_4)\cos\phi)\cos\theta \\ &\quad +(-I_3 + I_4)\cos\zeta\sin\phi\sin\theta\big]\sin\zeta\sin\phi \\ M_{13} &= -(A + (I_3 - I_4)\cos\phi)\sin\phi\sin\zeta \\ M_{14} &= (I_3 + A\cos\phi)\cos\zeta \\ M_{22} &= \frac{I_1}{2} - \frac{I_1}{2}\cos(2\theta) + (I_2 + I_3\sin^2\phi)\cos^2\theta \\ &\quad +I_4\cos^2\zeta\sin^2\phi\sin^2\theta \\ &\quad +(I_4\cos^2\theta + I_3\cos^2\zeta\sin^2\theta)\cos^2\phi \\ &\quad +A\cos\zeta\sin\phi\sin(2\theta) \\ &\quad +(A - A\cos^2\theta + A\sin^2\theta \\ &\quad +(I_3 - I_4)\cos\zeta\sin\phi\sin(2\theta))\cos\phi \\ &\quad +I_3\sin^2\theta\sin^2\zeta \\ M_{23} &= (I_2 + I_4\cos^2\phi + I_3\sin^2\phi)\cos\theta \\ &\quad +(A + (I_3 - I_4)\cos\phi)\cos\zeta\sin\phi\sin\theta \\ M_{24} &= (I_3 + A\cos\phi)\sin\theta\sin\zeta \\ M_{33} &= I_2 + I_4\cos^2\phi + I_3\sin^2\phi \\ M_{34} &= 0 \\ M_{44} &= I_3 \end{aligned}$$

and $M_{ij} = M_{ji}$. The constants I_1, I_2, I_3, A are defined in the text.

References

Abramowitz M, Stegun IA (1972) Orthogonal polynomials. In: Handbook of mathematical functions with formulas, graphs, and mathematical tables. Dover, New York

Asada H, Slotine JJE (1986) Robot analysis and control. Wiley, New York

Biess A (2001) Multijoint point-to-point arm movements of humans in 3d-space: minimum kinetic energy paths. In: Proceed tenth biennal conference International Graphonomics Society, University of Nijmegen, pp 142–146

Biess A (2004) Deterministic and stochastic computational modelling approaches to point-to-point arm movements. PhD Dissertation, The Weizmann Institute of Science, Rehovot, Israel

Bishop CM (1995) Neural networks for pattern recognition. Oxford University Press, New York

Bulirsch R (1971) Die Mehrzielmethode zur numerischen Lösung von nichtlinearen Randwertproblemen und Aufgaben der optimalen Steuerung Report R1.06, Carl-Cranz-Gesellschaft e.V., Deutsches Zentrum für Luft- und Raumfahrt (DLR), Oberpfaffenhofen, Germany

Flanders M, Hondzinski JM, Soechting JF, Jackson JC (2003) Using arm configurations to learn the effects of gyroscopses and other devices. J Neurophysiol 89:450–459

Flash T, Hogan N (1985) The coordination of arm movements: an experimentally confirmed mathematical model. J Neurosci 5:1688–1703

Fletcher R (2000) Practical methods of optimization. Wiley, New York

Galicki M (1995) Redundancy resolution of manipulator by global optimization. Appl Math Comp Sci 5:277–293

Gelfand IM, Fomin SV (1963) Calculus of variations. Prentice-Hall, New Jersey

Georgopoulus AP, Schwartz AB, Kettner RE (1986) Neuronal population coding of movement direction. Sience 233:1416–1419

Harris CM (1998) On the optimal control of behavior: a stochastic perspective. J Neurosci 83:73–88

Harris CM, Wolpert DM (1998) Signal-dependent noise determines motor planning. Nature 394:780–784

Kaneko Y, Nakano E, Osu R, Wada Y, Kawato M (2005) Trajectory formation based on the minimum commanded torque change model using the euler-poisson equation. Syst Comput Jpn 36:92–103

Keller HB (1968) Numerical methods for two-point boundary value problems. Blaisdell, Waltham

Laquaniti F, Terzuolo C, Viviani P (1983) The law relating the kinematics and figural aspects of drawing movemnts. Acta Psychol 54:115–130

Moran DW, Schwartz AB (1999) Motor cortical representation of speed and direction during reaching. J Neurophysiol 82:2676–2692

Nagurka ML, Yen V (1990) Fourier-based optimal control of nonlinear dynamic systems. ASME J Dyn Syst Meas Contr 112:17–26

Nakano E, Imamizu H, Osu R, Uno Y, Gomi H, Yoshioka T, Kawato M (1999) Quantitative examinations of internal representations for arm trajectory planning: minimum commanded torque change model. J Neurophysiol 81:2140–2155

Nishikawa KC, Murray ST, Flanders M (1999) Do arm postures vary with the speed of reaching? J Neurophysiol 81:2582–2586

Nocedal J, Wright S (1999) Numerical optimization. Springer, Berlin Heidelberg, New York

Richardson MJE, Flash T (2000) On the emulation of natural movements by humanoid robots. Humanoids, MIT, Cambridge

Richardson MJE, Flash T (2002) Comparing smooth arm movements with the two-thirds power law and the related segmented-control hypothesis. J Neurosci 22:8201–8211

Schaal S, Sternad D, Osu R, Kawato M (2004) Rhythmic arm movement is not discrete. Nat Neurosci 7:1137–1144

Shin KG, McKay MD (1986) Selection of near-minimum time geometric paths for robotic manipulators. IEEE Trans Auto Control 31:501–511

Soechting JF, Bueno CA, Hermann U, Flanders M (1995) Moving effortlessly in three dimensions: does Donders' law apply to arm movement. J Neurosci 15:6271–6280

Sosnik R, Hauptman B, Karni A, Flash T (2004) When practice leads to co-articulation: the evolution of geometrically defined movement primitives. Brain Res 156:422–438

Stoer J, Bulirsch R (1980) Introduction to numerical analysis. Springer, Berlin Heidelberg, New York

Todorov E, Jordan MJ (1998) Smoothness maximization along a predefined path accurately predicts the speed profiles of complex arm movements. J Neurophysiol 80:696–714

Todorov E, Jordan MI (2002) Optimal feedback control as a theory of motor coordination. Nat Neurosci 5:1226–1235

Torres EB, Zipser D (2002) Reaching to grasp with a multi-jointed arm. I. Computational model. J Neurophysiol 88:2355–2367

Torres EB, Zipser D (2004) Simultaneous control of hand displacements and rotations in orientation-matching experiments. J Appl Physiol 96:1978–1987.

Uno Y, Kawato M, Suzuki R (1989) Formation and control of optimal trajectory in human arm movement – minimum torque-change model. Biol Cybern 61:89–101

von Stryk O, Schlemmer M (1994) Optimal control of the industrial robot manutec r3. Comput Optim Control Int Ser Numer Math 115:367–382

Viviani P, Flash T (1995) Minimum-jerk, two-thirds power law, and isochrony. J Exp Psychol 6:828–845

Viviani P, Terzuolo C (1982) Trajectory determines movement dynamics. Neuroscience 7:431–437

Wada Y, Kaneko Y, Nakano E, Osu R, Kawato M (2001) Quantitaive examinations for multi joint arm trajectory planning – using a robust calculation algorithm of the minimum commanded torque change trajectory. Neural Netw 14:381–393

Wang X, Maurin M, Mazet F, de Castro Maia N, Voinot K, Verriest JP, Fayet M (1998) Three-dimensional modeling of the motion range of axial rotation of the upper arm. J Biomech 31:899–908

Yen V, Nagurka ML (1988) A suboptimal trajectory planning algorithm for robotic manipulators. ISA Trans 27:51–59